Spatial and temporal organization of RecA in the *Escherichia coli* DNA-damage response

Harshad Ghodke[1,2], Bishnu P Paudel[1,2], Jacob S Lewis[1,2], Slobodan Jergic[1,2], Kamya Gopal[3], Zachary J Romero[3], Elizabeth A Wood[3], Roger Woodgate[4], Michael M Cox[3], Antoine M van Oijen[1,2*]

[1]School of Chemistry, University of Wollongong, Wollongong, Australia

[2] Illawarra Health and Medical Research Institute, Wollongong, Australia

[3] Biochemistry Department, University of Wisconsin-Madison, Madison, Wisconsin, United States of America

[4] Laboratory of Genomic Integrity, National Institute of Child Health and Human Development, National Institutes of Health, Bethesda, MD, USA

Correspondence:

Antoine M van Oijen, School of Chemistry, University of Wollongong, Wollongong, New South Wales, 2522, Australia

Lead contact:

Antoine M van Oijen, School of Chemistry, University of Wollongong, Wollongong, New South Wales, 2522, Australia

Summary:

The RecA protein orchestrates the cellular response to DNA damage via its multiple roles in the bacterial SOS response. Lack of tools that provide unambiguous access to the various RecA states within the cell have prevented understanding of the spatial and temporal changes in RecA structure/function that underlie control of the damage response. Here, we develop a monomeric C-terminal fragment of the λ repressor as a novel fluorescent probe that specifically interacts with RecA filaments on single-stranded DNA (RecA*). Single-molecule imaging techniques in live cells demonstrate that RecA is largely sequestered in storage structures during normal metabolism. Upon DNA damage, the storage structures dissolve and the cytosolic pool of RecA rapidly nucleates to form early SOS-signaling complexes, maturing into DNA-bound RecA bundles at later time points. Both before and after SOS induction, RecA* largely appears at locations distal from replisomes. Upon completion of repair, RecA storage structures reform.

Introduction

All cells possess an intricately regulated response to DNA damage. Bacteria have evolved an extensive regulatory network called the SOS response to control the synthesis of factors that

protect and repair the genome. Processes coordinately regulated within the SOS response include error-free DNA repair, error-prone lesion bypass, cell division, and recombination.

The RecA protein is the master regulator of SOS, with at least three distinct roles. First, RecA forms a ternary complex with single-stranded DNA (ssDNA) and ATP to form the activated RecA*. RecA* catalyzes auto-proteolysis of the transcriptional repressor LexA to induce expression of more than 40 SOS genes (Courcelle et al., 2001; Fernandez De Henestrosa et al., 2000; Kenyon and Walker, 1980; Little and Mount, 1982; Little et al., 1981). RecA* thus uses the ssDNA generated when replication forks encounter DNA lesions as an induction signal (Sassanfar and Roberts, 1990). Second, along with several other accessory proteins, RecA mediates error-free recombinational DNA repair at sites of single-strand gaps, double-strand breaks (DSBs) and failed replisomes (Cox et al., 2000; Kowalczykowski, 2000; Kuzminov, 1995; Lusetti and Cox, 2002). Third, the formation and activity of active DNA Polymerase V complex capable of lesion bypass requires RecA* (Jaszczur et al., 2016; Jiang et al., 2009; Robinson et al., 2015).

RecA is a prototypical member of a class of proteins that are critical for genomic stability across all domains of life (Baumann et al., 1996; Bianco et al., 1998; Lusetti et al., 2003a; San Filippo et al., 2008; Sung, 1994). In higher organisms, including humans, the homologous protein Rad51 supports error-free double-strand break repair by catalyzing strand exchange much like the RecA protein does in eubacteria (Baumann et al., 1996; Sung, 1994). Mutations in human Rad51 and accessory proteins have been implicated in carcinomas and Fanconi anemia (Chen et al., 2015; Kato et al., 2000; Prakash et al., 2015). Unsurprisingly, RecA and related recombinases are highly regulated, with a variety of accessory proteins governing every facet of their multiple functions (Cox, 2007). Directed-evolution approaches can be used to enhance the catalytic activities of recombinases in cells (Kim et al., 2015). However, RecA functional enhancement has a cost, disrupting an evolved balance between the various processes of DNA metabolism that share a common genomic DNA substrate (Kim et al., 2015). Many deleterious genomic events occur at the interfaces between replication, repair, recombination, and transcription.

An understanding of how organisms maintain genetic integrity requires an examination of the protein actors in their native cellular environments. In response to DNA damage, transcription of the *recA* gene is upregulated ten-fold within minutes (Courcelle et al., 2001; Renzette et al., 2005). Using immunostaining, the copy number of RecA in undamaged cells has been estimated to be about 7,000-15,000 per cell, increasing to 100,000 per cell upon triggering the DNA-damage response (Boudsocq et al., 1997; Stohl et al., 2003). Visualization of C-terminal GFP fusions of wild-type and mutant *recA* alleles placed under the native *recA* promoter in *E. coli* have revealed that RecA forms foci in cells (Lesterlin et al., 2014; Renzette et al., 2005; Renzette et al., 2007). Interpretation of the localizations observed in these experiments has been clouded by three issues: 1. fluorescent fusions of RecA have consistently yielded loss-of-function phenotypes to RecA (Handa et al., 2009; Renzette et al.,

2005), making interpretation of the localizations revealed by these tagged proteins highly challenging. 2. this issue is further complicated by the fact that fluorescent proteins do not behave as inert tags and can influence intracellular localization in bacterial cells (Ghodke et al., 2016; Ouzounov et al., 2016). Indeed, *Bacillus subtilis* RecA tagged with GFP, YFP and mRFP yielded different localizations in response to DNA damage (Kidane and Graumann, 2005). These challenges do not come as a surprise since both N- and C-terminal ends are important for RecA function and localization (Eggler et al., 2003; Lusetti et al., 2003a; Lusetti et al., 2003b; Rajendram et al., 2015). 3. at least *in vitro*, untagged RecA has a remarkable ability to self-assemble, into different complexes that form on single-stranded DNA (RecA*), on double-stranded DNA, or are free of DNA (Brenner et al., 1988; Egelman and Stasiak, 1986, 1988; Stasiak and Egelman, 1986). The properties of these assemblies are often determined by the state of hydrolysis of associated ATP. Thus, unambiguous assignment of the molecular composition of RecA features in live cells has been difficult.

In the absence of DNA, RecA can polymerize to form aggregates of various stoichiometry to yield dimers, tetramers, 'rods' and 'bundles' (Brenner et al., 1988). Some of these states may have a physiological relevance: RecA fusions with the best functionality have revealed DNA-free aggregates that are confined to the cellular poles, outside of the nucleoid and associated with anionic phospholipids in the inner membrane (Rajendram et al., 2015; Renzette et al., 2005). These DNA-free aggregates were hypothesized to be 'storage structures' of RecA, although their functionality in and relevance to the DNA damage response remain unclear.

Early electron-microscopy studies revealed that multiple dsDNA-RecA-ATPγS filaments could also associate to form structures confusingly termed as 'bundles' (Egelman and Stasiak, 1988). This study also identified that ssDNA-RecA-ATPγS filaments could aggregate together. Electron microscopy of cells revealed that RecA appeared to form 'bundles' that were aligned next to the inner membrane in cells after DNA damage (Levin-Zaidman et al., 2000). In cells carrying an additional allele of wild-type RecA at a secondary chromosomal locus to increase overall RecA function, long RecA structures called 'bundles' were formed during double-strand break repair (Lesterlin et al., 2014). These bundles are similar to RecA structures called 'threads', that nucleate at engineered double-strand breaks in *Bacillus subtilis* (Kidane and Graumann, 2005). RecA bundles form after SOS induction by other means than double-strand breaks, and also then interact with anionic phospholipids in the inner membrane (Garvey et al., 1985; Rajendram et al., 2015). The appearance of elongated RecA* foci after treatment with UV has not always been associated with bundle formation (Renzette et al., 2007). It should be noted that whereas assemblies of RecA observed *in vivo* have been variously referred to as filaments, threads or bundles, their correspondence to the *in vitro* observations of RecA aggregates referred to as 'rods' or 'bundles' remains unclear.

Due to the similar morphology of the fluorescence signal arising from these various DNA-bound repair or DNA-free storage structures, teasing out dynamics of individual repair complexes in live cells has proven difficult. The limited functionality of RecA fusion proteins

112 utilized to date also raises concerns about the relationship of the observed structures to
113 normal RecA function. Several fundamental questions remain unanswered: When and where
114 does SOS signaling occur in cells? How is excess RecA stored?

115 In this work, we describe the development of a probe that specifically visualizes RecA
116 structures on DNA, and utilize it as part of a broader effort to provide a detailed time line of
117 RecA structural organization in living cells after DNA damage. With the objective of selectively
118 localizing DNA-bound and ATP-activated RecA* as a key repair intermediate inside living cells,
119 we produced a monomeric, catalytically dead N-terminal truncation of the bacteriophage λ
120 repressor CI (mCI*; CI 101-229, A152T, P158T, K192A*) that retains the ability to bind RecA-
121 ssDNA filaments. Removal of the N-terminal domain renders the mCI unable to bind DNA,
122 leaving only RecA* as a binding partner. Using both untagged and fluorescently labelled mCI
123 constructs, we document the effects of mCI *in vitro* and *in vivo*. We use mCI as well as the
124 most functional RecA-GFP fusion protein variants to distinguish between the various types of
125 RecA structures and follow their behavior through time. In addition, we examine the location
126 of RecA* foci formed in the nucleoid in relation to the location of the cellular replisomes. Our
127 results reveal how the activity of RecA is regulated upon triggering of the SOS pathway and
128 identify the various states of RecA that are relevant throughout the damage response.

129 **Results**

130 **RecA-GFP forms different types of aggregates in cells**

131 Damage in the template strand can result in the stalling or decoupling of replication, leading
132 to the accumulation of single-stranded DNA. This ssDNA provides a RecA nucleation site to
133 form RecA*, the structure that amplifies the cellular signal for genetic instability (Figure 1A).
134 In response to DNA damage, transcription of the SOS-inducible genes is up-regulated. Because
135 production of RecA occurs rapidly after damage, it is critical to observe live cells at early time
136 points with high temporal resolution after SOS induction.

137 With the objective of characterizing the spatial and temporal organization of RecA in cells
138 during SOS induction, we performed time-lapse imaging of individual *E. coli* cells immobilized
139 in flow cells using a variety of fluorescent probes (See SI for imaging methods). This setup
140 enabled us to monitor growing cells with nutrient flow at 30°C, while keeping the cells in place
141 to support long-term, time-lapse imaging of individual cells. A quartz window in the flow cell
142 enabled us to provide *in situ* UV irradiation with a defined dose (20 Jm^{-2}) at the start of the
143 experiment. Following this, we monitored fluorescence every 5 minutes over the course of
144 three hours by wide-field acquisition (Figure 1B). For this study we chose to induce SOS with
145 UV for two key reasons: first, UV light is a strong inducer of the SOS response, and second, a
146 pulse of UV light serves to synchronize the DNA damage response in cells that are
147 continuously replicating DNA without the need for additional synchronization.

148 First, we set out to characterize the temporal activity of the *recA* promoter alone in wild-type
149 MG1655 cells in response to ultraviolet radiation. We imaged cells that express fast-folding
150 GFP from the *gfpmut2* gene placed under the *recA* promoter on a low-copy reporter plasmid,
151 with a maturation time of less than 5 minutes ('pRecAp-gfp' cells; strain# HG260) (Kalir et al.,
152 2001; Zaslaver et al., 2006). The copy number of this reporter plasmid has been shown to
153 remain unchanged in response to ultraviolet radiation (Ronen et al., 2002). The cells retain
154 the chromosomal copy of the wild type *recA* gene. Measurements of the mean fluorescence
155 intensity of cytosolic GFP in pRecAp-gfp cells exhibited a gradual increase peaking at
156 approximately 135 min, with a maximum that corresponded to a two-fold increase compared
157 to the initial fluorescence intensity (SI Movie 1 & Figure 1C). After UV exposure, the
158 accumulation of the fluorescent reporter protein expressed from the *recA* promoter reaches
159 a maximum only after more than two hours. By extension, this gradual increase is used here
160 to define the time period during which cellular RecA concentration is increasing after UV
161 treatment.

162 Next, we imaged MG1655 cells that carry a *recA-gfp* fusion allele expressed from the
163 *recAo1403* operator in place of the wild-type chromosomal copy of *recA* ('*recA-gfp*' cells;
164 strain# HG195). The *recAo1403* promoter increases the basal (non-SOS) level of *recA*
165 expression by a factor of 2-3 (Rajendram et al., 2015; Renzette et al., 2005). Despite the higher
166 expression level, cells expressing this RecA-GFP fusion protein are deficient in RecA functions;
167 notably, these cells exhibit a three-fold lower survival in response to UV irradiation, and ten-
168 fold lower ability to perform recombination (Renzette et al., 2005). Additionally, these cells
169 exhibit delayed kinetics of SOS induction, but are still able to induce the SOS response to the
170 same extent as wild-type cells (Renzette et al., 2005). In response to UV irradiation, GFP
171 fluorescence in *recA-gfp* cells increased after DNA damage and peaked at approximately 130
172 min (SI Movie2 & Figure 1C & 1D). Thus, the kinetics of the observed increase in the levels of
173 chromosomally expressed RecA-GFP fusion protein are the same those of the increase seen
174 with the plasmid-based *gfpmut2* reporter under control of the *recA* promoter.

175 Measurements of the abundance of the *recA* transcript after SOS induction have revealed a
176 ten-fold increase within minutes after irradiation with UV (Courcelle et al., 2001). In bulk
177 experiments, the amount of RecA protein has been shown to attain a maximum at 90 min
178 after introduction of damage (Salles and Paoletti, 1983). Results from our live-cell
179 experiments are generally consistent with these studies, revealing that the amount of RecA
180 accumulated in cells attains a maximum at a time after triggering the SOS response that is
181 much later than the de-repression of the *recA* promoter. During the SOS response, many cells
182 undergo filamentation as cell division is blocked while some DNA synthesis continues
183 (Howard-Flanders et al., 1968). The increase in gene expression counters the dilution in the
184 cellular RecA concentration that is caused by the filamentation of the cells.

185 In these experiments, RecA-GFP formed well-defined features both before and after DNA
186 damage (SI Movie 2 and Figure 1D). These foci exhibited various morphologies ranging from

punctate foci to bundles. The foci became generally larger and more abundant after UV irradiation. To determine whether RecA foci formed in the absence of DNA damage are functionally distinct from those formed during the SOS response, we set out to specifically visualize RecA*, the complex that is formed when RecA binds ssDNA and that is actively participating in repair. To that end, we investigated interaction partners of the ssDNA-RecA filament that are not endogenously present in *E. coli*. Since the MG1655 strain we use in our studies is cured of bacteriophage λ, we focused on co-opting the λ repressor to detect RecA* in cells (Figure 1E) (Roberts and Roberts, 1975).

The monomeric C-terminal fragment of the bacteriophage λ repressor (mCI) stabilizes dynamics of RecA-ssDNA filaments *in vitro*

The bacteriophage λ repressor CI is responsible for the maintenance of lysogeny in *E. coli* infected with phage λ (Echols and Green, 1971). Oligomers of CI bind the operator regions in the constitutive P_L and P_R promoters in λ DNA and inhibit transcription from these promoters (Ptashne et al., 1980). In response to DNA damage, the λ repressor CI exhibits RecA* dependent auto-proteolysis, much like the homologous proteins in bacteria, LexA and UmuD (Burckhardt et al., 1988; Ferentz et al., 1997; Luo et al., 2001; Roberts and Roberts, 1975; Stayrook et al., 2008; Walker, 2001). In this reaction, the ssDNA-RecA filament (RecA*) stabilizes a proteolysis-competent conformation of CI enabling auto-proteolysis at Ala111-Gly112 (Ndjonka and Bell, 2006; Sauer et al., 1982). This co-protease activity of the RecA* filament results in loss of lysogeny due to de-repression of transcription of *cI* and prophage induction of λ. The N-terminal DNA-binding domain of CI is dispensable for interactions with RecA*(Gimble and Sauer, 1989). A minimal C-terminal fragment of the λ repressor CI(101-229 A152T P158T K192A) (henceforth referred to as mCI, Molecular weight 14307.23 Da; Figure 1F) efficiently inhibits the auto-catalytic cleavage of a hyper-cleavable monomeric C-terminal fragment CI(92-229) (Ndjonka and Bell, 2006). Cryo-electron microscopy has revealed that the mCI binds deep in the groove of the RecA filament (Galkin et al., 2009).

Given the existing extensive *in vitro* characterization of mCI, we decided to further develop it as a probe for detecting RecA* in cells. To better understand the kinetics, cooperativity and affinity of mCI for RecA-ssDNA filaments, we first pursued an *in vitro* investigation of the interaction between mCI and RecA filaments. Additionally, to visualize mCI in live-cell experiments, we made fusion constructs with fluorescent proteins tagged to the N terminus of mCI via a 14-amino acid linker. To perform time-lapse imaging, we tagged mCI with the yellow fluorescent protein YPet, and to perform live-cell photoactivatable light microscopy (PALM), we tagged mCI with the photoactivatable red fluorescent protein PAmCherry. Untagged mCI and the two fluorescently labelled constructs, PAmCherry-mCI and YPet-mCI were purified and characterized for RecA-ssDNA binding as described below (See SI for details, SI Figure 1A).

Binding of the mCI constructs to ssDNA-RecA filaments was first assayed by surface plasmon resonance (SPR). We immobilized a 5' biotinylated $(dT)_{71}$ ssDNA substrate on the surface of a

226 streptavidin-functionalized SPR chip (Figure 2A) and assembled RecA-ssDNA filaments by
227 injecting 1 µM RecA in buffer supplemented with ATP. This was followed by injection of buffer
228 without RecA, but supplemented with ATPγS to minimize disassembly of the RecA filament
229 on the ssDNA immobilized on the chip surface (SI Figure 1B). Next, the experiment was
230 repeated but now introducing to pre-formed RecA* filaments solutions that not only contain
231 stabilizing ATPγS, but also either untagged or fluorescently tagged mCI proteins. Figure 2B
232 shows scaled sensorgrams that are corrected for any disassembly of the ssDNA-RecA-ATPγS
233 filament and thus reporting on interactions of mCI with the highly stable RecA* filament (see
234 also SI Figure 1C). These sensorgrams reveal that mCI associates with the RecA filament in a
235 biphasic manner. Dissociation of mCI from the RecA filament was slow, with a dissociation
236 halftime ($t_{1/2}$) of 850 s. In comparison, the fluorescently tagged constructs dissociated faster,
237 but still slowly enough for use as a probe for the detection of RecA*. We measured a $t_{1/2}$ =
238 260 s and 280 s for YPet-mCI and PAmCherry-mCI respectively.

239 To probe the influence of mCI binding on the conformational state of the RecA* filament, we
240 next studied association of mCI with ssDNA-RecA-ATP filaments using single-molecule Förster
241 Resonance Energy Transfer (FRET) experiments. We used a previously described DNA
242 substrate consisting of a biotinylated 18-mer double-stranded region preceded by a 5' $(dT)_{40}$
243 overhang ('bio-ds18-$(dT)_{40}$', See SI for details, Figure 2C) (Park et al., 2010). This substrate
244 represents the partly single-stranded and partly double-stranded nature of the DNA substrate
245 that is thought to be generated in the context of replisomes encountering lesions *in vivo*. The
246 ssDNA region is labelled with a Cy3 donor probe on one end and a Cy5 acceptor probe on the
247 other so that the degree of extension of the ssDNA can be measured by FRET. The DNA
248 substrate was immobilized on a streptavidin-coated surface in a flow cell and the Cy5 FRET
249 signal was measured upon excitation of the Cy3 dye with a 532-nm laser (see SI for details).
250 Consistent with previous FRET investigations of this DNA substrate (Park et al., 2010), the DNA
251 substrate alone exhibited a FRET distribution with a mean value of 0.43 ± 0.07 (mean ±
252 standard deviation of a single Gaussian fit to the data) reflecting the ability of the ssDNA
253 overhang to entropically collapse and sample a large number of conformational states (Figure
254 2C, 2G & 2I; see 'DNA' trace). In the presence of ATP and RecA, the resulting FRET distribution
255 exhibited a peak with a mean FRET value of 0.3 ± 0.1, consistent with the formation of a highly
256 dynamic RecA filament undergoing simultaneous assembly and disassembly (Figure 2D, 2G
257 and 2I 'ATP' trace). Upon incubating the DNA substrate with RecA in the presence of ATPγS,
258 we observed a shift in the FRET distribution to an even lower value of 0.2 ± 0.07, reflecting
259 the formation of a rigid, fully extended ssDNA-RecA filament (Figure 2E, 2G and 2I 'ATPγS').
260 Since ATPγS traps the RecA filament in an 'active' conformation that is capable of LexA
261 repressor autocatalytic cleavage, we interpreted the 0.2 FRET state as corresponding to the
262 active state (Craig and Roberts, 1981). Incubation of RecA with ADP revealed a broad FRET
263 distribution similar to that obtained in the presence of ATP, reflecting unstable RecA filaments
264 assembled on the DNA overhang (See SI Figure 2A).

265 Next, we studied the FRET displayed by the ssDNA-RecA-ATP filament while titrating in
266 purified mCI (Figure 2H and SI Figure 2B) to gain insight into the influence of mCI binding on
267 the stability of ssDNA-RecA-ATP filaments (Figure 2F). In the presence of mCI the FRET
268 substrate exhibited a bi-modal behavior: either molecules exhibited the 0.43 FRET state or
269 the 0.2 FRET state. Upon increasing mCI concentration, the FRET distribution gradually shifted
270 from a mean of 0.43 to 0.2 in response to higher concentrations of mCI (Figure 2H). By fitting
271 the distributions to a sum of two Gaussian fits reflecting the 'bound' state (0.2 FRET) and
272 'unbound' state (0.4 FRET), we were able to obtain the bound fraction at every concentration
273 of mCI tested (Figure 2H and 2J). Fitting these data to the Hill equation yielded an equilibrium
274 dissociation constant of 36 ± 10 nM with a Hill coefficient of 2.4 ± 0.2 (Figure 2J). The increase
275 in the population of molecules in the lowest FRET state in response to an increase in mCI
276 concentration demonstrates that mCI stabilizes the RecA filament in the active conformation.

277 Examination of the FRET traces revealed that in the presence of mCI, the DNA substrate
278 exhibits stochastic transitions from the RecA-bound to the unbound state (e.g., Figure 2I for
279 [mCI] = 10 nM). The frequency of these transitions to the unbound state decreased in the
280 presence of high concentration of mCI (Figure 2I, see also SI Figure 2B). FRET traces of DNA
281 substrates in the presence of RecA and saturating concentrations of mCI (3 μM) exhibited
282 stable, long-lived binding events at a FRET value of 0.2 over the time scale of acquisition
283 (Figure 2G). To obtain off rates from the data, we applied a threshold of 0.3 (SI Figure 2C) to
284 segment the trajectories such that segments with FRET values less than 0.3 were considered
285 to reflect the 'bound' state, and those above 0.3 were considered to be the 'unbound' state.
286 The cumulative residence time distributions for the binding events (low FRET values) in the
287 FRET trajectories were best fit by a sum of two exponentials decaying according to a fast off
288 rate $k_{off,1}$ = 0.23 ± 0.06 s^{-1} and a slow off rate $k_{off,2}$ = 0.044 ± 0.002 s^{-1} (Figure 2K). These off-
289 rates were largely independent of the concentration of mCI (Figure 2K). However, strikingly,
290 the fraction of the population decaying following the slower off rate increased from 35% in
291 the absence of mCI to 91% in the presence of 1μM mCI (Figure2L).

292 Next we probed the influence of mCI on the ability of RecA* to perform three key catalytic
293 functions *in vitro*: LexA cleavage, ATP hydrolysis and strand-exchange. Incubation of pre-
294 formed RecA* filaments on circular ssDNA M13mp18 substrates with micromolar
295 concentrations of mCI revealed a pronounced inhibition of RecA* ATPase activity (SI Figure
296 2D). The tagged mCI variants did not significantly inhibit RecA* ATPase activity at
297 concentrations under 500 nM (SI Figure 2D). Monitoring of LexA cleavage by RecA* in the
298 presence of mCI revealed that even high concentrations of mCI did not inhibit LexA cleavage,
299 at best, mCI at micromolar concentrations slowed the kinetics of LexA cleavage
300 (Supplementary Fig. 2E). Finally, whereas strand-exchange by RecA* was potently inhibited
301 at micromolar concentrations of mCI (Supplementary Fig. 2F), tagged mCI constructs did not
302 significantly inhibit strand-exchange activity at concentrations below 500 nM (Supplementary
303 Fig. 2F).

304 Taken together, these *in vitro* investigations provide insights into the consequences of mCI
305 binding on the activity of RecA*. We found that mCI stabilizes the RecA* filament in the
306 'active' conformation that is capable of LexA cleavage. At high concentrations (5 – 10 µM),
307 mCI can inhibit ATP hydrolysis and strand-exchange by RecA*, and delay LexA cleavage. This
308 is consistent with mCI binding to the RecA nucleoprotein filament groove as anticipated.
309 Importantly, at low concentrations (10 - 100 nM) similar to those we eventually employed as
310 a standard in vivo (as described below), these key activities of RecA* are not significantly
311 affected by the presence of mCI or tagged variant. These findings emphasize the suitability of
312 the use of mCI derived probes for probing RecA* function.

313 **mCI inhibits SOS induction in a concentration-dependent manner**

314 We probed whether mCI interacts with ssDNA-RecA filaments (RecA*) in cells upon DNA
315 damage and potentially inhibits the SOS response. To that end, we created live-cell imaging
316 vectors that express either mCI or the PAmCherry-mCI fusion from the *araBAD* promoter in a
317 tunable manner depending on the amount of L-arabinose provided in the growth medium
318 (Guzman et al., 1995). The ability of cells to induce SOS was assayed using a previously
319 described set of SOS-reporter plasmids that express GFP in response to DNA damage (Zaslaver
320 et al., 2006). In this assay, we measured the fluorescence of fast-folding GFP expressed from
321 the *gfpmut2* gene under the SOS-inducible *sulA* promoter on a low-copy plasmid ('*sulAp-*
322 *gfp*')(Zaslaver et al., 2006). As a control, we also measured GFP fluorescence from the
323 promoter-less parent vector ('*gfp*'). The copy number of these SOS-reporter plasmids is not
324 influenced by the ultraviolet radiation (Ronen et al., 2002). To measure the ability of mCI to
325 inhibit the SOS response in cells, we co-transformed wild-type MG1655 cells with either the
326 pBAD-mCI vector ('*mcI*'), pBAD-PAmCherry-mCI vector ('*PAmCherry-mcI*') or an empty pBAD
327 vector ('pBAD'), and *sulA* reporter ('*sulAp-gfp*') or promoter-less vector ('*gfp*') to generate
328 four strains: 1. cells that carry the empty pBAD vector and the promoter-less *gfp* vector
329 ('*gfp*+pBAD', strain# HG257) 2. cells that carry the empty pBAD vector and the *sulA* reporter
330 plasmid ('*sulAp-gfp* + pBAD', strain# HG258) 3. cells that carry the pBAD-mCI vector and the
331 *sulA* reporter plasmid ('*sulAp-gfp* + *mcI*', strain# HG253) and 4. cells that carry the pBAD-
332 PAmCherry-mCI vector and the SOS-reporter plasmid ('*sulAp-gfp + PAmCherry-mcI*', strain#
333 HG285).

334 We then acquired time-lapse movies of these cells to observe the evolution of the SOS
335 response over three hours after UV damage (Figure 3A). As expected, when cells carrying the
336 *sulA* reporter plasmid and the empty pBAD vector ('*sulAp-gfp* + pBAD') were irradiated with
337 a 20 Jm^{-2} dose of UV, we observed a robust increase in GFP fluorescence (Figure 3A; strain#
338 HG258). In contrast, cells carrying the promoter-less control vector and the empty pBAD
339 vector ('*gfp*+pBAD') vectors did not exhibit any increase in GFP fluorescence in response to
340 UV (Figure 3A, summarized in Figure 3C; strain# HG257).

341 After these experiments confirming the robustness of the *sulA* reporter as a readout for SOS
342 induction, we grew cells carrying both the *sulA* reporter and the mCI vectors ('*sulAp-gfp* +

343 *mcI*', strain# HG253) in imaging medium containing 0, 10^{-3} or 10^{-2} % L-arabinose and
344 immobilized them in flow cells. In this L-arabinose concentration regime, we expect the mCI
345 copy number to be approximately 20, 50 and 500 copies per cell, respectively (Ghodke et al.,
346 2016). Time-lapse acquisition after UV irradiation revealed that SOS induction was sensitive
347 to the presence of mCI. Even leaky expression of mCI caused a measurable delay in GFP
348 fluorescence (Figure 3A). This delay was found to be proportional to the expression level of
349 mCI, and cells grown in 10^{-2} % L-arabinose exhibited nearly complete inhibition of SOS
350 induction during the experimental timeline of three hours after UV irradiation (Figure 3A and
351 3C). Time-lapsed imaging of wild-type cells carrying the pBAD-PAmCherry-mCI vector and the
352 *sulA* reporter plasmid ('*sulAp-gfp* + *PAmCherry-mcI*', strain# HG285) also revealed a similar
353 delay in SOS induction depending on the concentration of L-arabinose in the growth medium
354 (Figure 3B). These data suggest that mCI competes with LexA in cells at sites of RecA* in
355 response to DNA damage.

356

357 **Most RecA filaments are formed at sites distal to replisomes after DNA damage**

358 A long-standing model for SOS induction predicts that RecA* filaments are formed on
359 chromosomal DNA when replisomes encounter UV lesions (Sassanfar and Roberts, 1990).
360 These RecA* filaments are believed to be the sites of SOS induction. While several lines of
361 evidence support the model that RecA* filaments are formed after UV irradiation, direct
362 visualization in living *E. coli* cells has not been demonstrated. Given that mCI robustly interacts
363 with RecA* filaments, we set out to visualize RecA* in cells exposed to UV light. Importantly,
364 considering that mCI can inhibit RecA* activities at µM concentrations, we chose to express
365 mCI variants from the tightly repressed, and tunable pBAD promoter. Incubating cells with
366 low concentrations of L-arabinose results in cells expressing tagged mCI constructs in the 10-
367 100 nM range in cells.

368 This was achieved by imaging a two-color strain that expresses a chromosomal YPet fusion of
369 the *dnaQ* gene (that encodes the replisomal protein ϵ, a subunit of the replicative DNA
370 polymerase III), and PAmCherry-mCI from the pBAD-PAmCherry-mCI plasmid in the presence
371 of L-arabinose (strain# HG267). The YPet fusion has previously been shown to minimally affect
372 the function of ϵ (Reyes-Lamothe et al., 2010; Robinson et al., 2015). The two-color strain was
373 grown in medium containing small amounts of L-arabinose ($5x10^{-4}$ %) to induce low
374 expression of PAmCherry-mCI. Under these conditions, UV-surivival of HG267 was
375 indistinguishable from that of MG1655/pBAD-mycHisB(strain# HG116) (SI Figure 3A).This was
376 followed by time-lapse imaging (5 min intervals for 3 h after 20 Jm^{-2} of UV) in flow-cells. In
377 this experiment, we performed live-cell PALM to detect PAmCherry-mCI, and TIRF imaging to
378 detect replisomes (see SI for technical details related to imaging, SI Figure 3B). This approach
379 enabled us to visualize replisomes as well as mCI foci (Figure 4A). To compare cells in the
380 presence and absence of SOS induction, we carried out the same experiments in cells carrying
381 the *lexA3*(Ind^-) allele (strain# HG311; Figure 3C). These cells express a non-cleavable mutant

382 of the LexA repressor (G85D) that binds RecA*, but fails to induce SOS (Figure 4A and B)
383 (Markham et al., 1981).

384 SOS induction resulted in an increase in mCI/RecA foci. In the absence of DNA damage, 19%
385 of all *lexA*$^+$ cells exhibited at least one PAmCherry-mCI focus (Figure 4A and 4C (green line), *t*
386 = -5 min; summarized in Figure 4H). In response to UV damage inflicted at *t* = 0 min, we
387 detected an increase in the number of *lexA*$^+$ cells with at least one PAmCherry focus to 56%
388 of the population at *t* = 60 min after UV (green line, Figure 4C, total numbers for each time
389 point are presented in SI Figure 3C). The number of replisome foci detected per cell was found
390 to remain relatively constant ranging from 3.5 ± 0.14 (mean ± standard error) in the absence
391 of UV to 4.2 ± 0.2 per cell at *t* = 60 min after UV (blue line, Figure 4D). The number of
392 PAmCherry-mCI foci marking sites of RecA* was found to increase approximately five-fold
393 from 0.3 ± 0.15 per cell before UV irradiation to 1.4 ± 0.25 per cell at *t* = 60 min (red line,
394 Figure 4D). Among cells exhibiting at least one focus, 24 ± 8% (mean ± standard error) of
395 PAmCherry-mCI foci co-localized with replisomes before UV irradiation, and this number
396 increased to 34 ± 5% at 60 min after UV (Figure 4F and 4I).

397 Blocking SOS induction also limited RecA/mCI focus formation. Only 1.5% of the *lexA3*(Ind$^-$)
398 (gray line Figure 4C) population exhibited at least one PAmCherry-mCI focus (compared to
399 19% for wild-type) (summarized in Figure 4H) in the absence of UV. Additionally, the number
400 of PAmCherry-mCI foci detected remained consistently low, with 0.28 ± 0.17 foci per cell
401 compared to *lexA*$^+$ cells (compare red lines in Figure 4E and 4D), suggesting that the inability
402 to cleave LexA results in an absence of available binding sites for PAmCherry-mCI. Strikingly,
403 *lexA3*(Ind$^-$) cells did not exhibit PAmCherry-mCI foci that co-localized with replisomes before
404 UV irradiation (Figure 4G). At 60 minutes after UV irradiation, only 21% of the population
405 exhibited PAmCherry-mCI foci compared to 56% in case of the wild-type (Figure 4C, 4H). Of
406 these, 32 ± 11% of the PAmCherry-mCI foci co-localized with replisomes at 60 minutes (Figure
407 4G, 4I). These results are consistent with the model that some RecA* filaments are formed in
408 cells in the vicinity of replisomes when cells are exposed to UV light. Most RecA* filaments
409 are formed at locations distal to the replisome.

410 14 ± 5% of the replisomes exhibited co-localization with mCI in *lexA*$^+$ cells exhibiting
411 PAmCherry-mCI foci (Figure 4F). These results suggest that in approximately twenty percent
412 of the population RecA filaments are formed during normal growth (Figure 4C, 'No UV' time
413 point). However only approximately 24% of these are associated with replisomes (blue line,
414 Figure 4F, 'No UV' time point). These RecA* filaments formed at sites of replisomes in the
415 absence of UV light might reflect replication forks engaged in recombination-dependent DNA
416 restart pathways or replication forks stalled at sites of bulky endogenous DNA damage. In
417 contrast, fewer *lexA3*(Ind$^-$) cells exhibited PAmCherry-mCI foci suggesting that the non-
418 cleavable LexA(G85D) protein competes with mCI for the same substrates *in vivo*. These
419 results reinforce our observations that mCI and LexA compete for the same binding substrates
420 *in vivo.*

421 **RecA forms bundles that are stained by mCI in cells**

422 Previous studies have noted the formation of large macromolecular assemblies of RecA in
423 response to double-strand breaks in cells (Lesterlin et al., 2014). These aggregates of RecA-
424 GFP have been termed 'bundles' (Figure 1C and references (Lesterlin et al., 2014; Rajendram
425 et al., 2015)). Our experiments with MG1655/pBAD-PAmCherry-mcI also revealed
426 localizations of mCI that resembled RecA bundles (Figure 5A). These observations were also
427 reproduced in cells expressing YPet-mCI from a pBAD plasmid (strain# HG143). Cells were
428 induced with 10^{-3} % L-arabinose, immobilized in flow cells, irradiated with a dose of 20 Jm^{-2} of
429 UV, and imaged using a time-lapse acquisition protocol. In this experiment, YPet-mCI initially
430 exhibits cytosolic localization at the start of the experiment (Figure 5B, t = -5 min ('No UV'
431 time point)) and reveals foci and bundles at later time points (Figure 5B, t = 1 h and 2 h).

432 Next, we tested whether the formation of these bundles required RecA that has wild-type
433 functions. To that end, we imaged YPet-mCI in DH5α cells that carry the *recA1* allele (an
434 inactive mutant, G160D) (Bryant, 1988). These cells did not exhibit foci or bundles that bound
435 to YPet-mCI after UV (Figure 5C, strain# HG242). These data demonstrate that mCI recognizes
436 a specific configuration of wild-type RecA on ssDNA – one that is able to co-operatively bind
437 and hydrolyze ATP.

438 The UvrD helicase performs a critical role in disassembling RecA filaments in cells (Centore
439 and Sandler, 2007; Lestini and Michel, 2007; Petrova et al., 2015; Veaute et al., 2005). Since
440 mCI stabilizes RecA-ssDNA filaments *in vitro*, we hypothesized that persistent RecA* filaments
441 would lead to constitutive SOS in Δ*uvrD* cells lacking the ability to disassemble RecA*. To test
442 this hypothesis, we imaged Δ*uvrD* cells (strain# HG235) expressing plasmid-based YPet-mCI
443 and found that these cells indeed exhibited constitutive RecA bundles. The presence of
444 constitutive SOS in these cells is further confirmed by the observation of a strong
445 filamentation, even in the absence of any external DNA damage (SI Figure 4).

446 Taken together, these results demonstrate that: 1) RecA bundles are not only formed by
447 RecA-GFP but also by wild-type RecA during the SOS response and 2) The ability to form a
448 high-affinity complex on ssDNA is critical for the formation of RecA bundles. Further, the lack
449 of mCI features in the *recA1* background suggest that far from being DNA-free aggregates of
450 RecA, these bundles contain an ordered assembly of RecA that is bound to DNA.

451 **RecA forms storage structures that are not stained by mCI**

452 We then turned our attention to focus on how RecA is stored in cells. Storage structures of
453 RecA would need to satisfy two criteria to be distinguished from complexes active in DNA
454 repair and from polar aggregates representing mis-folded proteins: 1) the size or number of
455 these structures should be proportional to the amount of RecA present in the cell and 2) RecA
456 stored in these structures should be available for biological function when required, that is,
457 after DNA damage. To detect storage structures of RecA in live cells, we imaged *recA-gfp* cells

458 in the absence of DNA damage (strain# HG195). Cells exhibited punctate foci that appear to
459 be positioned outside the nucleoid (Figure 6A). Since the cells did not exhibit additional
460 markers of distress, namely cell filamentation, we presumed that the RecA features
461 correspond to storage structures of RecA. We hypothesized that the size of these punctate
462 foci is dependent on the copy number of RecA in cells. To test this hypothesis, we pursued a
463 strategy involving over-expression of unlabeled RecA from a plasmid in *recA-gfp* cells and
464 measuring whether the foci become larger as the amount of untagged RecA increases and
465 integrates into the structures with the labelled RecA.

466 To that end, we created plasmids that expressed wild type RecA protein at two different
467 levels. First, a low-copy plasmid expressed *recA* from the constitutive *recAo281* operator
468 (pConst-RecA; see SI for details) (Uhlin et al., 1982; Volkert et al., 1976). A second version of
469 that plasmid (pG353C-RecA) cut expression in half by incorporating an altered ribosome
470 binding site (RBS) (see SI Figure 5A). We then imaged *recA-gfp* cells carrying one or the other
471 of these plasmids. Time-lapsed imaging of undamaged cells (5 min intervals for 3h) revealed
472 that the RecA-GFP signal was confined to a single large feature (Figure 6A). To quantify the
473 size of RecA features in the absence of DNA damage, we measured the maximum Feret
474 diameter (referring to the largest physical dimension of the structure; Figure 6A) of the
475 feature at a threshold above the background (Figure 6B, see SI for details). Comparison of the
476 Feret diameters of features in *recA-gfp* cells carrying the pConst-RecA and pG353C-RecA
477 vectors revealed a strong dependence on the expression level of untagged wild-type RecA
478 protein (Figure 6B). *recA-gfp*/pConst-RecA cells exhibited larger features than *recA-*
479 *gfp*/pG353C-RecA cells or *recA-gfp* cells alone. Notably, the storage structures exhibited
480 cross-sections that were circular (in the case of *recA-gfp cells)* or elliptical (in the case of *recA-*
481 gfp/pConst-RecA or *recA-gfp/*pG353C-RecA cells) unlike the previously described thread-like
482 filamentous RecA-bundles (Kidane and Graumann, 2005; Lesterlin et al., 2014). In the absence
483 of DNA damage, these structures were stably maintained in cells in *recA-gfp*/pG353c-RecA
484 cells (SI movie 3). Upon cell division, these structures were disproportionately inherited by
485 daughter cells. Notably, cells did not exhibit markers of distress consistent with induction of
486 SOS, suggesting that these storage structures do not impede DNA replication during growth,
487 and are likely not assembled on DNA. Since the presence and size of these features is
488 dependent on the amount of RecA present in cells, henceforth we refer to them as a 'storage
489 structures'.

490 To exclude the possibility that RecA-GFP storage structures are artefacts of the GFP fusion,
491 we collected electron-microscopy images of immunogold-stained RecA in four genetic
492 backgrounds: 1) Δ*recA*; 2) wild-type MG1655; 3) MG1655/pConst-RecA; and 4) *recA-*
493 *gfp*/pConst-RecA (Figure 6 panels C-F, respectively). As expected, clusters of gold-labelled
494 RecA antibodies could be observed in all samples except Δ*recA* cells (Figure 6C). Cells carrying
495 the over-expresser plasmid pConst-RecA exhibited strong RecA staining that was localized to
496 the membrane (Figure 6E, 6F. See SI Figure 5B for additional examples). These results support

497 the conclusion that excess RecA is stored in the form of membrane-associated, storage
498 structures even in cells carrying untagged, wild-type RecA.

499 Stored RecA should be made available to support repair during the SOS response. We tested
500 this hypothesis by exposing *recA-gfp*/pG353C-RecA cells to ultraviolet radiation and
501 monitoring the dynamics of the storage structures in time-lapsed fashion. We found that the
502 storage structures dissolve within one hour after introducing damage, flooding the cell with
503 RecA-GFP (Figure 6G, t = 1 h). At later time points, the storage structures re-appeared at
504 locations close to the poles (Figure 6G, t = 2 h 45), suggesting that the RecA is stored away
505 until needed (see also SI Movie 4). We characterized the dynamics of storage structure
506 disassembly by plotting the cumulative probability of loss of storage structures for the
507 population of cells that possessed a distinct storage structure as a function of time (Figure 6H;
508 orange curve). We found that for *recA-gfp*/pG353C-RecA cells, half of the storage structures
509 were lost within 45 $\pm$ 5 min after UV damage (see SI for details). We then plotted the
510 cumulative probability distribution of time of appearance of storage structures after SOS
511 induction (Figure 6H, green curve). In these cells, half of the population of storage structures
512 that formed after UV damage, did so after 135 $\pm$ 5 minutes after UV.

513 Next, we investigated whether mCI interacts with these storage structures. Fluorescence
514 imaging of plasmid-based YPet-mCI expressed from the pBAD promoter in wild-type cells
515 expressing pG353C-RecA (strain# HG446) did not reveal any morphological features
516 consistent with those of the storage structures observed in *recA-gfp*/pG353C-RecA cells. YPet-
517 mCI was found to be cytosolic in the absence of DNA damage, suggesting a lack of stable
518 association with RecA storage structures (Figure 6I, 'No UV' time point). As noted earlier, foci
519 were rare. As described before, in response to UV irradiation, cytosolic YPet-mCI was found
520 to form foci and bundles (Figure 6I, 120 min time point; see also SI Movie 4). These results
521 suggested that YPet-mCI does not interact with RecA storage structures. Observations of cells
522 expressing plasmid-based mCI in *recA-gfp*/pG353C-RecA revealed no detectable influence of
523 mCI on the morphology of these structures (SI Figure 5C), reinforcing the interpretation that
524 mCI does not interact with storage structures of RecA in the absence of damage.

525 To further confirm that storage structures are indeed distinct from RecA bundles, we
526 characterized the kinetics of RecA-GFP bundle formation in *recA-gfp* cells (strain# HG195). In
527 these cells, RecA storage structures are small (Figure 6A) and indistinguishable from repair
528 foci. Upon UV irradiation, cytosolic RecA-GFP forms foci that progress to form large, cell-
529 spanning bundles over the course of several tens of minutes (see SI Movie2), unlike RecA
530 storage structures observed in the *recA-gfp*/pG353C-RecA cells. Plotting a cumulative
531 probability distribution of time of incidence of bundle formation revealed that half of all
532 bundles in *recA-gfp* cells appear by 60 minutes after UV (Figure 6H, red curve). This timing is
533 consistent with measurements of incidence of bundle formation during double-strand break
534 repair (Lesterlin et al., 2014).

535 **DinI promotes the formation of storage structures in cells**

536 The DinI protein is a modulator of RecA function (Lusetti et al., 2004a; Lusetti et al., 2004b;
537 Renzette et al., 2007). In solution, the C-terminal tail of DinI mimics ssDNA, enabling
538 interactions with monomeric RecA (Ramirez et al., 2000). Since free RecA assembles to form
539 storage structures, we next investigated whether storage of RecA was influenced by DinI.
540 Considering that expression level of RecA influences storage structure formation, we first
541 constructed a strain carrying the *recA-gfp* chromosomal fusion under its native wild-type
542 promoter (P_{wt}-*recA-gfp*; strain# EAW428). We deleted *dinI* in this background (strain#
543 EAW767). In the absence of DNA damage, we detected storage structures in fewer Δ*dinI* cells
544 (27% of 702 cells) compared to *dinI*$^+$ cells (43% of 855 cells). Additionally, these structures
545 were smaller (see Figure 6J). Over-expression of DinI from pBAD-DinI in Δ*dinI* cells further
546 confirmed this result: cells recovered storage structures in the presence of L-arabinose (see
547 SI Figure 5D). These findings suggest that RecA storage structure formation may be promoted
548 by DinI.

549 **Discussion**

550 In this work, we have used the C-terminal fragment of the λ repressor in conjunction with
551 single-molecule imaging techniques in live cells to examine RecA protein dynamics in
552 response to SOS induction. In the absence of DNA damage, we see that RecA is largely
553 sequestered in storage structures. Upon UV irradiation, these storage structures dissolve and
554 the cytosolic pool of RecA rapidly nucleates to form early SOS signaling complexes, followed
555 by RecA bundle formation at later time points. Our analysis indicates that the bundles are
556 bound to DNA and may be single extended RecA nucleoprotein filaments. Upon completion
557 of repair, RecA storage structures reform. Our use of the mCI reagent, which associates with
558 DNA-bound and activated RecA* complexes, allows us to eliminate the ambiguity associated
559 with earlier observations utilizing RecA fusion proteins with limited functionality and for the
560 first time provide access to the spatial and temporal behavior of the various forms of RecA
561 structures within the cell. In addition, whereas some RecA foci that form after DNA damage
562 co-localize with replisomes, the majority do not.

563 We set out to use binding partners of RecA to probe intracellular localization of SOS-signaling
564 RecA complexes. Several proteins associated with the SOS response, notably LexA, UmuD,
565 and the λ repressor, interact with RecA* to effect autocatalytic cleavage. The interaction of
566 these proteins with the activated RecA nucleoprotein filament has been a subject of intense
567 investigation (Cohen et al., 1981; Gimble and Sauer, 1985; Little, 1982). Even though each of
568 these proteins interacts with a different set of residues on the RecA* filament, they all occupy
569 the helical groove of the RecA filament prior to auto-proteolysis (Frank et al., 2000; Galkin et
570 al., 2009; Yu and Egelman, 1993). We sought to exploit this key feature by using a
571 fluorescently labelled C-terminal fragment of λ repressor CI (denoted mCI) to visualize RecA-
572 DNA complexes. The mCI construct binds specifically to RecA* (Figure 2, SI Figure1). Binding
573 of mCI stabilizes RecA* in the 'active' conformation capable of mediating transcription-factor
574 cleavage, exhibiting an equilibrium dissociation constant of 36 ± 10 nM and a Hill coefficient

575 of 2.4 ± 0.2 for the binding of mCI to ssDNA-RecA filaments assembled on a dT_{40} ssDNA
576 overhang. Based on previous findings that one mCI contacts two RecA monomers, we
577 estimate that up to six mCI molecules can decorate the RecA-ssDNA filament composed of up
578 to 13 RecA monomers on the dT_{40} DNA substrate under conditions of saturating mCI
579 concentration (Galkin et al., 2009; Ndjonka and Bell, 2006). The non-cleavable mCI thus can
580 decorate RecA filaments assembled on DNA. We confirmed that mCI interacts with RecA
581 filaments in live cells by probing SOS induction after UV damage (Figure 3). We found that
582 mCI has the potential to robustly inhibit SOS induction at high concentrations. SOS induction
583 is retained, albeit delayed, at mCI concentrations employed in this study.

584 The leading model for SOS induction is that replication forks fail at sites of lesions and produce
585 large tracts of ssDNA that templates nucleation of RecA filaments. Visualizing this model in
586 cells has been challenging due to the difficulties associated with co-localization of a high-
587 abundance protein (RecA) with a handful of replisomes. Our strategy involving fluorescently
588 tagged mCI enabled us to examine the location of RecA* foci in nucleoids relative to the
589 replisomes for the first time in *E coli*. We found that the average number of replisome foci did
590 not change after DNA damage, confirming that most replisomes are not disassembled after
591 UV (Figure 4). Live-cell PALM imaging of mCI revealed foci that depended on the presence of
592 wild-type RecA and DNA damage. Surprisingly, 20% of wild-type cells exhibited RecA* foci
593 during normal growth. However, only 24% of these co-localized with replisomes. The
594 remaining 76% of sites of RecA* detected during normal growth did not co-localize with
595 replisomes. Upon exposure to ultraviolet light, 56% of cells exhibited RecA* foci that were
596 visualized by mCI, with up to 35% of the RecA* foci co-localized with replisomes at 60 min in
597 rich media (Figure 4). A previous report on co-localization of RecA-GFP with DnaX-mCherry in
598 *Bacillus subtilis* growing in minimal media reported a basal co-localization of 74.8 ± 8.4 % with
599 an increase to 84.3 ± 5.8 % at 5 min after 40 Jm^{-2} UV treatment (Lenhart et al., 2014). The
600 extent of co-localization of RecA* and replisomes detected in our experiments, in *E coli* cells
601 growing in media that supports multi-fork replication is lower both before and after UV
602 irradiation. The RecA* foci that co-localize with replisomes are likely associated with
603 replisomes that are stalled at sites of DNA damage. We postulate that RecA* foci that are not
604 co-localizing with replisomes are forming in DNA gaps that are formed and left behind by the
605 replisome (Howard-Flanders et al., 1968; Rupp and Howard-Flanders, 1968; Yeeles and
606 Marians, 2013). Notably, most foci of the translesion DNA polymerases IV and V also form at
607 nucleoid locations that are distal from replisomes, both before and after SOS induction
608 (Henrikus et al., 2018; Robinson et al., 2015).

609 The large cell-spanning structures termed RecA threads or bundles (we have adopted the
610 latter term) (Kidane and Graumann, 2005; Lesterlin et al., 2014; Rajendram et al., 2015) that
611 form after SOS induction deserve special mention. Following the initial phase of RecA*
612 formation, cells expressing YPet-mCI, PAmCherry-mCI or RecA-GFP exhibited large RecA
613 bundles. The formation of these bundles was also contingent upon the presence of wild-type
614 RecA. The *recA1* allele in DH5α failed to support focus or bundle formation, consistent with

615 the inability of the RecA(G160D) in DH5α to induce SOS and HR functions (Bryant, 1988).
616 Additionally, cells lacking UvrD exhibited constitutive RecA bundles. These bundles are thus a
617 hallmark of the DNA damage response and may have special functionality in the homology
618 search required for recombinational DNA repair (Lesterlin et al., 2014). Here, we show that
619 the bundles bind to our mCI probe. This implies that the bundles are either bound to DNA and
620 thus activated as RecA*, or at a minimum are in a RecA*-like conformation that permits mCI
621 binding. Interestingly, despite the differences in the nature of the DNA damage inflicted, the
622 timing of RecA bundle formation in our UV experiments coincided closely with that of RecA
623 bundles observed upon induction of site specific double-strand breaks in the chromosome
624 (Lesterlin et al., 2014). The bundles may thus be nucleated by RecA binding to either gaps or
625 resected double strand breaks. At later time points, polymerization of RecA filaments
626 nucleated at ssDNA gaps could extend onto dsDNA, and manifest as bundles in our
627 experiments. RecA bundles also interact with anionic phospholipids in the inner membrane
628 (Rajendram et al., 2015). Notably, UmuC also localizes primarily at the inner-membrane upon
629 production and access to the nucleoid is regulated by the RecA* mediated UmuD cleavage
630 (Robinson et al., 2015). This transition occurs late in the SOS response (after 90 min), at a
631 time-point when most, if not all of the cells in the population exhibit RecA bundles. The
632 origins, maturation and additional catalytic roles of RecA bundles in the SOS response require
633 additional investigation.

634 Our experiments enable us to distinguish storage structures from SOS signaling complexes
635 and RecA bundles based on three qualities: 1. storage structures dissolve after UV damage
636 whereas RecA bundles are formed in response to DNA damage. 2. storage structures often
637 exhibit a polar localization, whereas RecA-bundles form along the cell length. 3. the SOS
638 signaling complexes and RecA bundles are visualized by binding to mCI, whereas the RecA
639 storage structures are not. Finally, we found that DinI promotes storage structure formation:
640 cytosolic RecA in normal growing cells was found to be sequestered in structures by simply
641 over-expressing DinI from a plasmid.

642 Taken together, these data for the first time provide a full picture of a process that was first
643 hypothesized by Story and co-workers in 1992 suggesting that RecA can undergo a phase
644 transition to form DNA-free assemblies in live cells and redistribute into the cytosol where it
645 becomes available for DNA-repair functions (Figure 7). Within a few minutes after
646 encountering bulky lesions, replication forks synthesize ssDNA substrates that are rapidly
647 coated by cytosolic RecA to form RecA*. These RecA* enable auto-proteolysis of LexA to
648 initiate the SOS response and increase the levels of cellular RecA protein. Meanwhile, storage
649 structures of RecA dissolve, making RecA available for biological functions. The RecA* foci
650 elongate over several hours into elaborate bundles that may have multiple functions. Finally,
651 excess RecA is sequestered away into storage structures approximately two hours after DNA
652 damage, after DNA repair is complete and normal growth is restored.

653 **Author contributions**

Conceptualization: H.G, M.M.C, and A.M.V.O.; Methodology: H.G. and A.M.V.O.; Formal Analysis and Software: H.G. and B.P., Investigation, H.G., B.P., J.L. S.J. and R.W.; Writing – Original Draft: H.G.; Writing – Review & Editing: H.G., M.M.C., R.W., and A.M.V.O.; Funding Acquisition: A.M.V.O.; Resources: E.A.W., R.W.; Supervision: A.M.V.O.

Acknowledgements

We thank Douglas Weibel for the MG1655 RecA-GFP strain. We thank the Alon lab for the SOS-reporter plasmids. We thank Amy McGrath and Celine Kelso for technical assistance with ESI-MS analyses of purified proteins. R.W. was supported by the NICHD/NIH Intramural Research Program. M.M.C is supported by NIH Grant GM32335. A.M.V.O. acknowledges support by the Australian Research Council (DP150100956 and FL140100027).

665 **Figure legends**

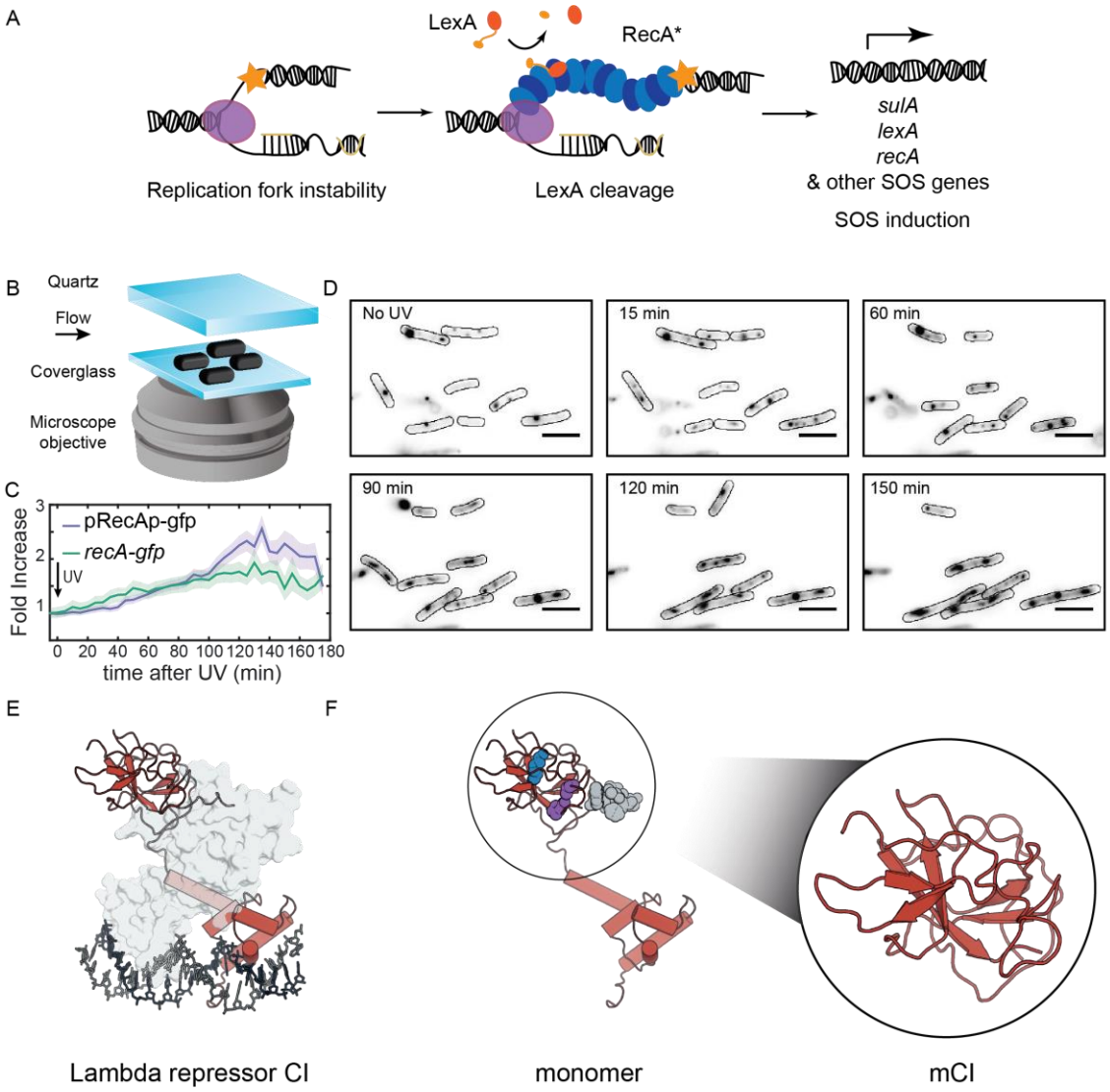

666

667 **Figure 1: RecA forms different intracellular structures in response to UV irradiation**

668 **A.** Consensus model for SOS induction after DNA damage, illustrating the formation of ssDNA-
669 containing RecA* filaments at sites of stalled replication forks. These RecA* filaments induce
670 the SOS response by promoting cleavage of LexA. **B.** Schematic of flow-cell setup for live-cell
671 imaging. **C.** Plots of relative increase in mean intensity of GFP in pRecAp-gfp *cells* (purple,
672 strain# HG260) or RecA-GFP expressed from the native chromosomal locus (*recA-gfp* cells).
673 Cells are irradiated with 20 Jm^{-2} of UV at t = 0 min. Shaded error bars represent standard error
674 of the mean cellular fluorescence measured in cells. 50 – 200 cells were analyzed at each time
675 point. Scale bar corresponds to 5 µm. See also SI Movie 1. **D.** Imaging of *recA-gfp* cells (strain#
676 HG195) reveals that RecA-GFP forms foci of various morphologies at different stages during
677 the SOS response. Stills from SI Movie 2 are presented here. **E.** Crystal structure of the
678 operator bound dimeric λ repressor CI (PDB ID: 3BDN). **F.** Monomer of CI showing the catalytic
679 lysine (K192, purple), residues that mediate dimerization (A152 and P158, blue), and the C

680 terminus involved in dimerization (grey). Inset shows the monomeric C-terminal fragment
681 'mCI' defined as CI(101-229, A152T P158A and K192A) used in this study.

682

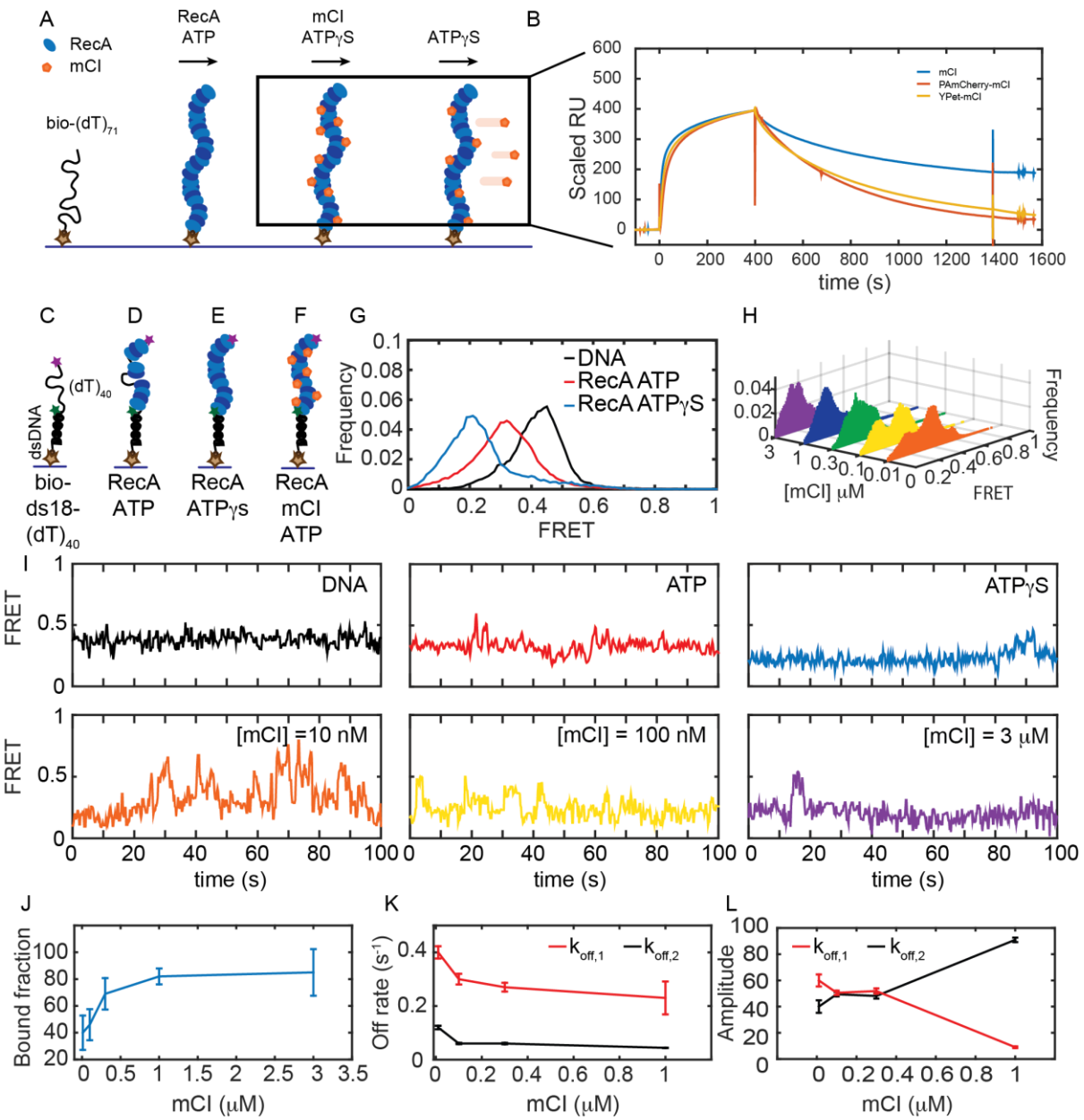

Figure 2: mCI stabilizes ssDNA-RecA filaments *in vitro*

A. Schematic of SPR experiment probing association and dissociation kinetics of mCI from ssDNA-RecA-ATPγS filaments on the surface of an SPR chip. ssDNA-RecA-ATPγS filaments were assembled on a biotinylated $(dT)_{71}$ ssDNA molecule. mCI, YPet-mCI or PAmCherry-mCI were then flowed into the flow cell at time t = 0 for 400 s to monitor the association phase. Dissociation of mCI from ssDNA-RecA-ATPγS filaments was observed by leaving out mCI from the injection buffer. **B.** Sensorgram reveals biphasic association of mCI to RecA filaments, followed by a slow dissociation from the ssDNA-RecA-ATPγS filament. Sensorgrams presented here are corrected for slow disassembly of the RecA-ATPγS filament, and data are scaled to the binding curve of YPet-mCI for purposes of illustration (see also SI Figure 1 for unscaled

694 data). **C.** Schematic of single-molecule FRET assay used to probe the influence of mCI binding
695 on the conformational state of the ssDNA-RecA-ATP filament assembled on a ssDNA $(dT)_{40}$
696 overhang. Biotinylated substrate DNA (bio-ds18-$(dT)_{40}$) was immobilized on a functionalized
697 coverslip via a streptavidin-biotin interaction. **D.** RecA binds the ssDNA overhang dynamically
698 to form a ssDNA-RecA filament. **E.** In the presence of ATPγS, RecA forms a stable filament. **F.**
699 Incubation with mCI leads to a RecA filament decorated with mCI. **G.** FRET distributions
700 observed from the substrate alone, with RecA-ATP and RecA-ATPγS. **H.** Titration of mCI shifts
701 the RecA-ATP distribution to that of the active filament. **I.** Example FRET traces of DNA
702 substrate alone or when bound to RecA in the presence of ATPγS, or when bound to RecA in
703 the presence of ATP and mCI (0, 10, 100, 300, 1000 and 3000 nM mCI) **J.** Fitting of the Hill
704 equation to the percentage of bound fraction as a function [mCI] reveals a K_D of 36 ± 10 nM
705 and a cooperativity of 2.4 ± 0.2 **K.** Off rates measured from binding of mCI to ssDNA-RecA-
706 ATP filaments. **L.** Percentage amplitude of the detected rate-constants as a function of [mCI]
707 reveals enrichment of the population decaying according to the slow off-rate as a function of
708 [mCI]. See also SI Figures 1 and 2.

709

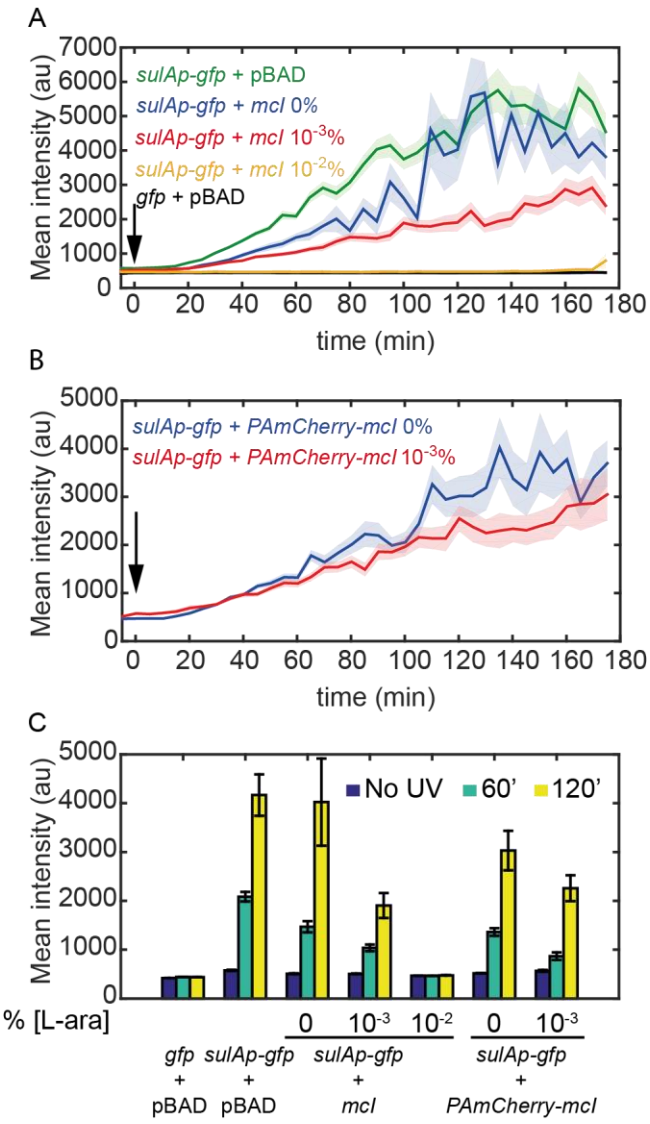

Figure 3: mCI inhibits the SOS response in a concentration-dependent manner

A. Time-lapse experiments were performed on MG1655 cells carrying the SOS-reporter plasmids ('*gfp*' or '*sulAp-gfp*') and pBAD-mCI plasmid ('*mcI*') following irradiation with 20 Jm^{-2} of UV-irradiation at time t = 0 min. Mean intensity of GFP fluorescence was measured in cells carrying the reporter plasmid and mCI or empty vector, and plotted here as follows: '*sulAp-gfp* + pBAD' cells (green; strain# HG258), '*gfp* + pBAD' cells (black; strain# HG257), '*sulAp-gfp* + *mcI*' (strain# HG253) (0% L-ara) (blue), 10^{-3} % L-ara (red) and 10^{-2} % L-ara (yellow), respectively. **B.** Mean intensity of GFP fluorescence in cells carrying the reporter plasmid and pBAD-PAmCherry-mCI plasmid ('*sulAp-gfp* + *PAmCherry-mcI*') (strain# HG285; 0% L-ara (blue) and 10^{-3} % L-ara (red)) is plotted as a function of time. Shaded error bars indicate standard error of mean cellular fluorescence for all cells imaged at the indicated time point. In these experiments, 50-200 cells were analyzed for each experiment for each of the 37 time points. **C.** Bar plots summarizing data presented in B and C under the indicated conditions at a time point before UV irradiation, one at 60, and one at 120 minutes after UV.

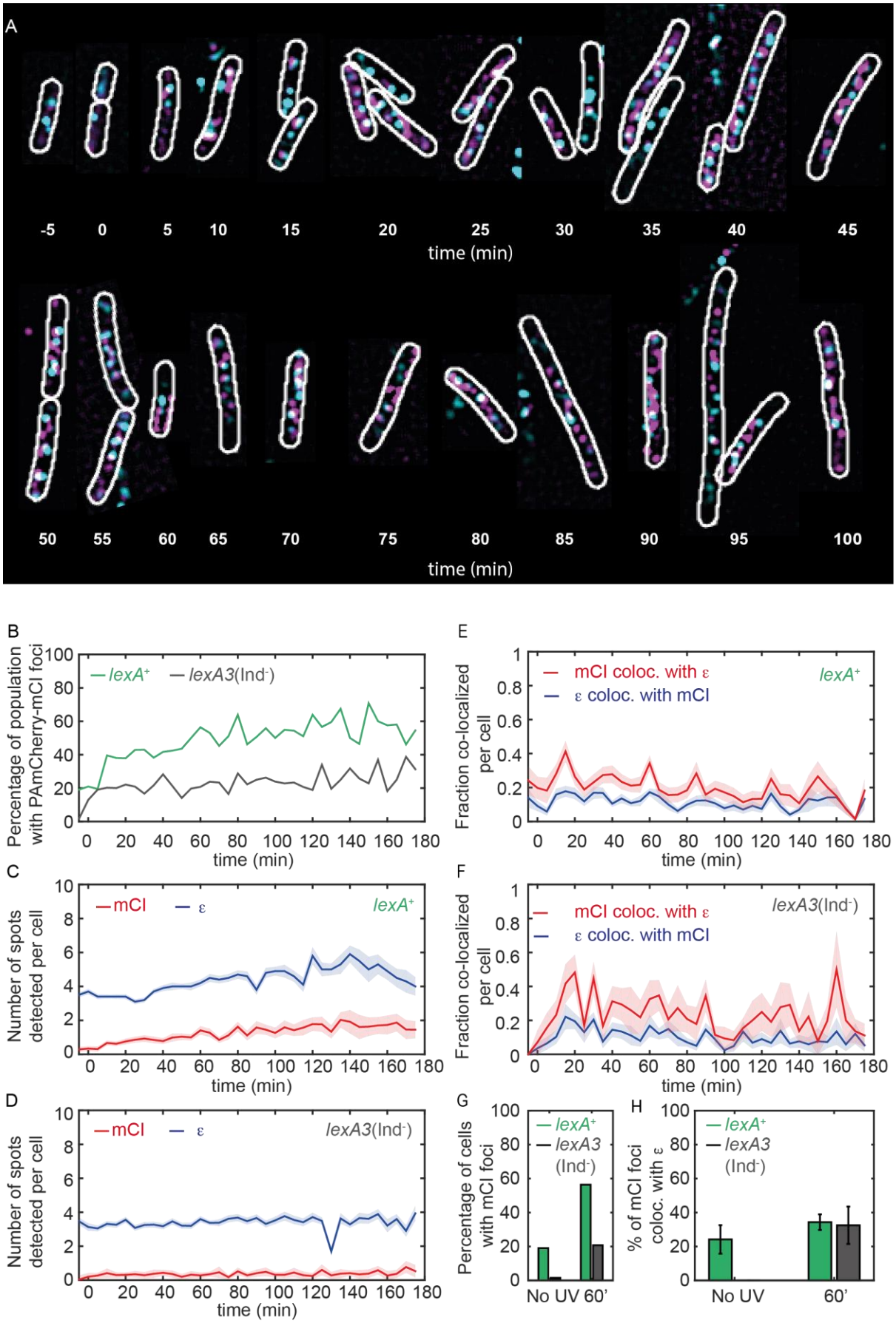

Figure 4: mCI co-localizes with the replisome after UV irradiation

727 MG1655 cells carrying the ϵ-YPet replisome marker and expressing plasmid PAmCherry-mCI
728 from pBAD-PAmCherry-mCI (strain# HG267) were grown in the presence of $5x10^{-4}$ % L-
729 arabinose and irradiated with 20 Jm^{-2} of UV-irradiation followed by imaging for three hours.
730 Examples of **A.** *lexA*$^{+}$ (strain# HG267) provided at indicated time points **B.** The percentage of
731 cells imaged at each time point with at least one PAmCherry-mCI focus is shown for *lexA*$^{+}$
732 (green) and *lexA3*(Ind^{-}) (black) cells. Number of replisome foci and PAmCherry foci were
733 counted for each time point per cell for **C**. *lexA*$^{+}$ and **D**. *lexA3*(Ind^{-}) cells. In cells exhibiting at
734 least one replisome focus and one PAmCherry-mCI focus, the fraction of replisomes co-
735 localizing with PAmCherry-mCI was determined (blue) and the fraction of PAmCherry-mCI co-
736 localizing with replisomes was determined (red) for **E.** *lexA*$^{+}$ and **F.** *lexA3*(Ind^{-}) cells. **G.** Bar
737 plots summarizing percentage of cells exhibiting at least one mCI focus for *lexA*$^{+}$ (green) and
738 *lexA3*(Ind^{-}) (gray) cells before UV and at 60 min after UV irradiation. **H.** Bar plots summarizing
739 extent of co-localization of ϵ-YPet and PAmCherry-mCI in cells with at least one mCI and ϵ
740 focus. Data are presented as mean ± SEM. 25-150 cells were analyzed for each time point
741 from at least three repeats of each experiment. See also SI Figure 3.

742

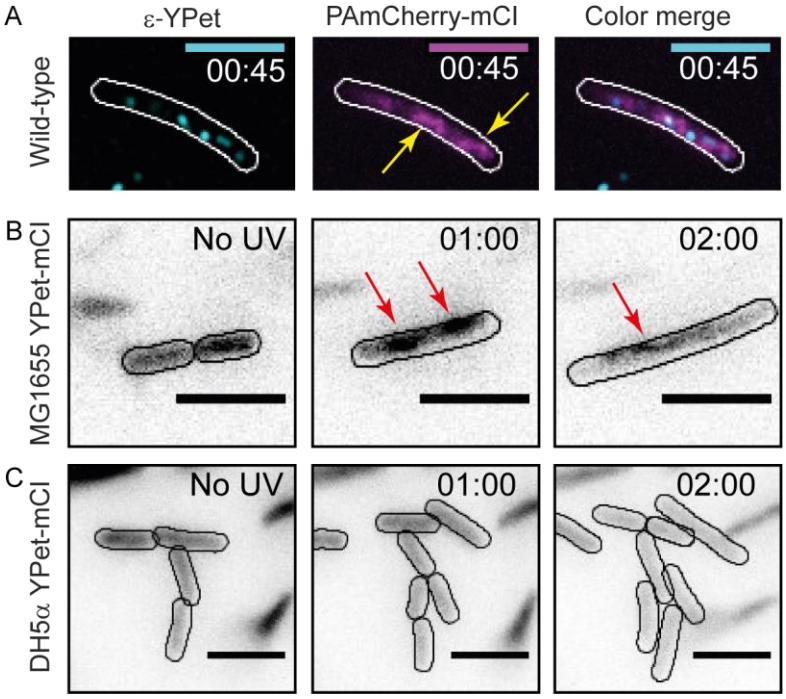

Figure 5: mCI stains RecA bundles after UV-damage

A. At late time points in the DNA damage response, PAmCherry-mCI forms large bundles in *recA*$^+$ cells. Shown here is an example of an overlay of the mCI signal (magenta) and replisomal ϵ foci (cyan) at t = 45 min after 20 Jm^{-2} UV. Yellow arrows point to RecA bundles. For purposes of illustration, peaks in the 514-nm ϵ channel were enhanced using a discoidal average filter. **B.** YPet-mCI also forms bundles (indicated by red arrows) in response to UV-damage in *recA*$^+$ cells. **C.** DH5α carrying the *recA1* allele does not exhibit foci or bundle formation upon UV-irradiation under identical conditions as in panel B. Scale bar corresponds to 5 µm. See also SI Figure 4. Cell outlines provided as a guide to the eye.

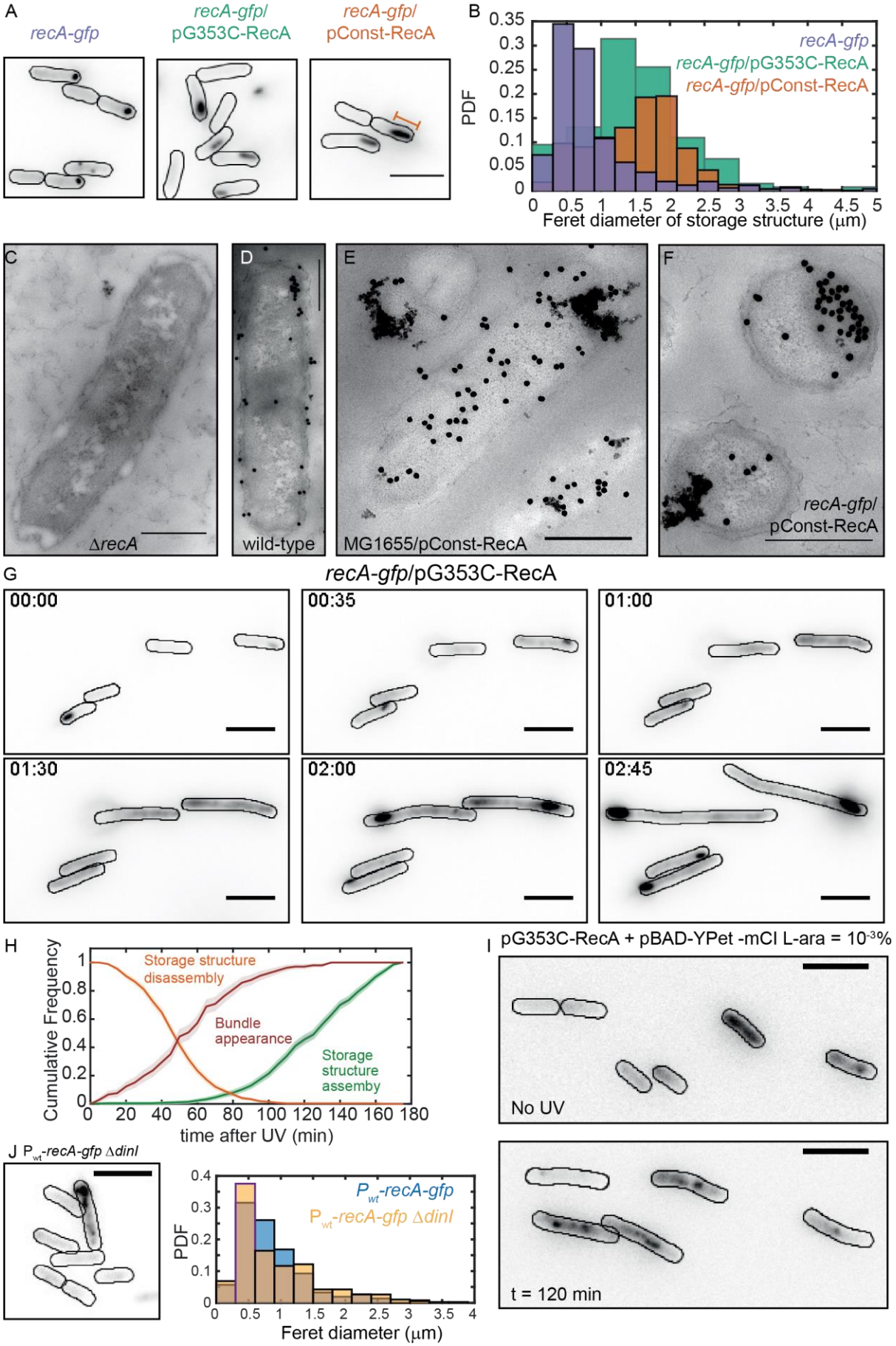
A
recA-gfp
recA-gfp/
pG353C-RecA
recA-gfp/
pConst-RecA
B
PDF
recA-gfp
recA-gfp/pG353C-RecA
recA-gfp/pConst-RecA
Feret diameter of storage structure (μm)
C
ΔrecA
D
wild-type
E
MG1655/pConst-RecA
F
recA-gfp/
pConst-RecA
G
recA-gfp/pG353C-RecA
00:00
00:35
01:00
01:30
02:00
02:45
H
Cumulative Frequency
Storage structure
disassembly
Bundle
appearance
Storage
structure
assemby
time after UV (min)
I
pG353C-RecA + pBAD-YPet -mCI L-ara = 10-3%
No UV
t = 120 min
J Pwt-recA-gfp ΔdinI
PDF
Pwt-recA-gfp
Pwt-recA-gfp ΔdinI
Feret diameter (μm)

754

755 **Figure 6: Excess RecA is stored in storage-structures**

756 **A.** Montage of *recA-gfp* (strain# HG195), *recA-gfp*/pG353C-RecA (strain# HG406) and *recA-*
757 *gfp*/pConst-RecA cells (strain# HG411) imaged in the absence of UV damage. See also SI Movie
758 3. **B.** Probability density functions of maximum Feret diameter of storage structures in *recA-*
759 *gfp* (purple), *recA-gfp*/pG353C-RecA (green) and *recA-gfp*/pConst-RecA (orange) cells. Orange
760 bar in panel A represents the maximum Feret diameter for that particular storage structure.
761 Electron microscopy images of **C**. Δ*recA* **D**. wild-type *recA* **E**. *recA-gfp*/pConst-RecA and **F**.
762 MG1655/pConst-RecA cells stained with gold nanoparticles labelled with RecA antibody. Note
763 the appearance of aggregates of gold nanoparticles at locations consistent with those
764 observed in panel A for *recA-gfp*/pConst-RecA cells (panel E). Untagged, over-expressed RecA
765 (F) reveals gold nanoparticle localizations consistent with those expected from RecA storage
766 structures. Scale bar corresponds to 1 µm. **G.** Montage of frames from a time-lapse
767 experiment of *recA-gfp*/pG353C-RecA cells exposed to UV (see also SI Movies 3 and 4). RecA
768 forms storage structures in the absence of DNA damage (0 min) in cells. Storage structures
769 dynamically dissolve after DNA damage (1 h). Storage structures reform by sequestering
770 excess RecA synthesized during SOS after repair (2 h and 2 h 45 min time points). **H.**
771 Cumulative probability distributions of time of solubilization of storage structure (yellow) and
772 time of appearance (light green) of storage structures from *recA-gfp*/pG353C-RecA (strain#
773 HG406) cells. Red line represents cumulative probability distribution of time of first incidence
774 of RecA bundles in *recA-gfp* cells (strain# HG195). Shaded error bars represent standard
775 deviation of the bootstrap distribution obtained by sampling 80% of the data 1,000 times. In
776 each case, 100-150 cells were analyzed that were present for the duration of observation (3
777 h). Scale bar represents 5 µm. **I.** YPet-mCI does not stain storage structures in
778 MG1655/pG353C-RecA pBAD-Ypet-mCI cells (strain# HG446) in the absence of DNA damage,
779 but forms features after UV damage (shown here is a still at 120 min). Cell outlines provided
780 as a guide to the eye. See also SI Movie 5, and SI Figure 5. **J.** MG1655 cells carrying the *recA-*
781 *gfp* fusion under the native *recA* promoter and Δ*dinI* (strain# EAW 767) exhibit fewer, and
782 smaller storage structures than *dinI*$^{+}$ cells.

783

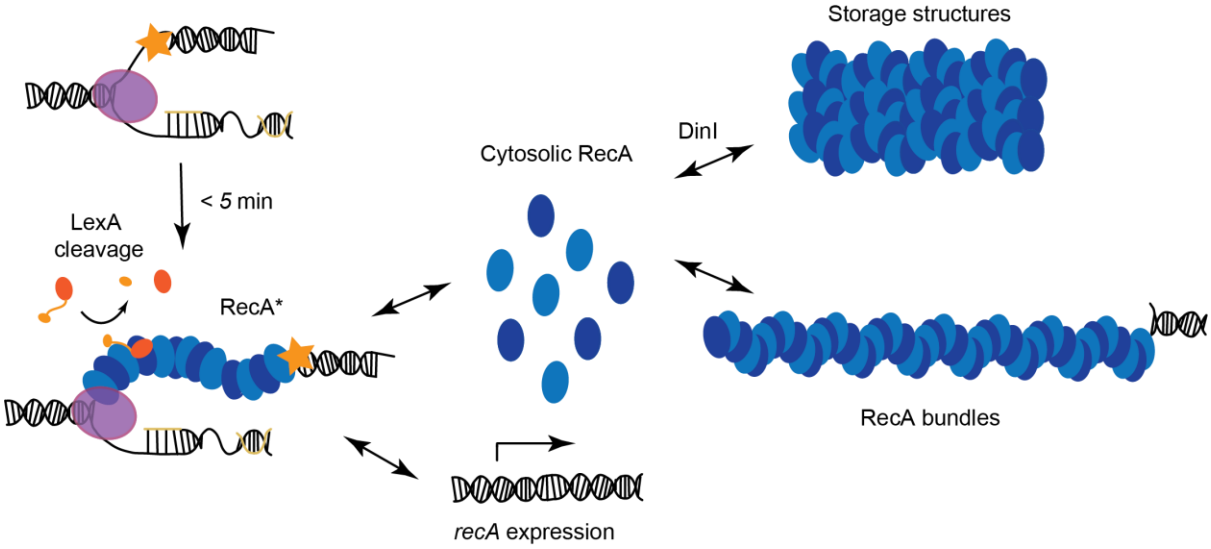

Figure 7: Model for organization of RecA complexes after DNA damage

Model for storage and re-distribution of RecA after DNA damage. Detection of UV damage leads to formation of ssDNA-RecA filaments at sites of replisomes. These ssDNA-RecA filaments catalyze auto-proteolysis of LexA to induce SOS and upregulate expression of RecA. Storage structures of RecA dissolve in response to DNA damage to make RecA available for repair and recombination.

References

Baumann, P., Benson, F.E., and West, S.C. (1996). Human Rad51 protein promotes ATP-dependent homologous pairing and strand transfer reactions in vitro. Cell *87*, 757-766.

Bianco, P.R., Tracy, R.B., and Kowalczykowski, S.C. (1998). DNA strand exchange proteins: a biochemical and physical comparison. Front Biosci *3*, D570-603.

Boudsocq, F., Campbell, M., Devoret, R., and Bailone, A. (1997). Quantitation of the inhibition of Hfr x F- recombination by the mutagenesis complex UmuD'C. J Mol Biol *270*, 201-211.

Brenner, S.L., Zlotnick, A., and Griffith, J.D. (1988). RecA protein self-assembly. Multiple discrete aggregation states. J Mol Biol *204*, 959-972.

Bryant, F.R. (1988). Construction of a recombinase-deficient mutant recA protein that retains single-stranded DNA-dependent ATPase activity. J Biol Chem *263*, 8716-8723.

Burckhardt, S.E., Woodgate, R., Scheuermann, R.H., and Echols, H. (1988). UmuD mutagenesis protein of Escherichia coli: overproduction, purification, and cleavage by RecA. Proc Natl Acad Sci U S A *85*, 1811-1815.

Centore, R.C., and Sandler, S.J. (2007). UvrD limits the number and intensities of RecA-green fluorescent protein structures in Escherichia coli K-12. Journal of bacteriology *189*, 2915-2920.

Chen, J., Morrical, M.D., Donigan, K.A., Weidhaas, J.B., Sweasy, J.B., Averill, A.M., Tomczak, J.A., and Morrical, S.W. (2015). Tumor-associated mutations in a conserved structural motif alter physical and biochemical properties of human RAD51 recombinase. Nucleic Acids Res *43*, 1098-1111.

Cohen, S., Knoll, B.J., Little, J.W., and Mount, D.W. (1981). Preferential cleavage of phage lambda repressor monomers by recA protease. Nature *294*, 182-184.

Courcelle, J., Khodursky, A., Peter, B., Brown, P.O., and Hanawalt, P.C. (2001). Comparative gene expression profiles following UV exposure in wild-type and SOS-deficient Escherichia coli. Genetics *158*, 41-64.

Cox, M.M. (2007). Regulation of bacterial RecA protein function. Crit Rev Biochem Mol Biol *42*, 41-63.

Cox, M.M., Goodman, M.F., Kreuzer, K.N., Sherratt, D.J., Sandler, S.J., and Marians, K.J. (2000). The importance of repairing stalled replication forks. Nature *404*, 37-41.

Craig, N.L., and Roberts, J.W. (1981). Function of nucleoside triphosphate and polynucleotide in Escherichia coli recA protein-directed cleavage of phage lambda repressor. J Biol Chem *256*, 8039-8044.

Echols, H., and Green, L. (1971). Establishment and maintenance of repression by bacteriophage lambda: the role of the cI, cII, and c3 proteins. Proc Natl Acad Sci U S A *68*, 2190-2194.

Egelman, E.H., and Stasiak, A. (1986). Structure of helical RecA-DNA complexes. Complexes formed in the presence of ATP-gamma-S or ATP. J Mol Biol *191*, 677-697.

Egelman, E.H., and Stasiak, A. (1988). Structure of helical RecA-DNA complexes. II. Local conformational changes visualized in bundles of RecA-ATP gamma S filaments. J Mol Biol *200*, 329-349.

Eggler, A.L., Lusetti, S.L., and Cox, M.M. (2003). The C terminus of the Escherichia coli RecA protein modulates the DNA binding competition with single-stranded DNA-binding protein. J Biol Chem *278*, 16389-16396.

Ferentz, A.E., Opperman, T., Walker, G.C., and Wagner, G. (1997). Dimerization of the UmuD' protein in solution and its implications for regulation of SOS mutagenesis. Nat Struct Biol *4*, 979-983.

Fernandez De Henestrosa, A.R., Ogi, T., Aoyagi, S., Chafin, D., Hayes, J.J., Ohmori, H., and Woodgate, R. (2000). Identification of additional genes belonging to the LexA regulon in Escherichia coli. Mol Microbiol *35*, 1560-1572.

Frank, E.G., Cheng, N., Do, C.C., Cerritelli, M.E., Bruck, I., Goodman, M.F., Egelman, E.H., Woodgate, R., and Steven, A.C. (2000). Visualization of two binding sites for the Escherichia coli UmuD'(2)C complex (DNA pol V) on RecA-ssDNA filaments. J Mol Biol *297*, 585-597.

Galkin, V.E., Yu, X., Bielnicki, J., Ndjonka, D., Bell, C.E., and Egelman, E.H. (2009). Cleavage of bacteriophage lambda cI repressor involves the RecA C-terminal domain. J Mol Biol *385*, 779-787.

841 Garvey, N., St John, A.C., and Witkin, E.M. (1985). Evidence for RecA protein association with the cell
842 membrane and for changes in the levels of major outer membrane proteins in SOS-induced
843 Escherichia coli cells. Journal of bacteriology *163*, 870-876.
844 Ghodke, H., Caldas, V.E., Punter, C.M., van Oijen, A.M., and Robinson, A. (2016). Single-Molecule
845 Specific Mislocalization of Red Fluorescent Proteins in Live Escherichia coli. Biophys J *111*, 25-27.
846 Gimble, F.S., and Sauer, R.T. (1985). Mutations in bacteriophage lambda repressor that prevent RecA-
847 mediated cleavage. Journal of bacteriology *162*, 147-154.
848 Gimble, F.S., and Sauer, R.T. (1989). Lambda repressor mutants that are better substrates for RecA-
849 mediated cleavage. J Mol Biol *206*, 29-39.
850 Guzman, L.M., Belin, D., Carson, M.J., and Beckwith, J. (1995). Tight regulation, modulation, and high-
851 level expression by vectors containing the arabinose PBAD promoter. Journal of bacteriology *177*,
852 4121-4130.
853 Handa, N., Amitani, I., Gumlaw, N., Sandler, S.J., and Kowalczykowski, S.C. (2009). Single molecule
854 analysis of a red fluorescent RecA protein reveals a defect in nucleoprotein filament nucleation that
855 relates to its reduced biological functions. J Biol Chem *284*, 18664-18673.
856 Henrikus, S.S., Wood, E.A., McDonald, J.P., Cox, M.M., Woodgate, R., Goodman, M.F., van Oijen, A.M.,
857 and Robinson, A. (2018). DNA polymerase IV primarily operates outside of DNA replication forks in
858 Escherichia coli. PLoS genetics *14*, e1007161.
859 Howard-Flanders, P., Rupp, W.D., Wilkins, B.M., and Cole, R.S. (1968). DNA replication and
860 recombination after UV irradiation. Cold Spring Harb Symp Quant Biol *33*, 195-207.
861 Jaszczur, M., Bertram, J.G., Robinson, A., van Oijen, A.M., Woodgate, R., Cox, M.M., and Goodman,
862 M.F. (2016). Mutations for Worse or Better: Low-Fidelity DNA Synthesis by SOS DNA Polymerase V Is
863 a Tightly Regulated Double-Edged Sword. Biochemistry *55*, 2309-2318.
864 Jiang, Q., Karata, K., Woodgate, R., Cox, M.M., and Goodman, M.F. (2009). The active form of DNA
865 polymerase V is UmuD'(2)C-RecA-ATP. Nature *460*, 359-363.
866 Kalir, S., McClure, J., Pabbaraju, K., Southward, C., Ronen, M., Leibler, S., Surette, M.G., and Alon, U.
867 (2001). Ordering genes in a flagella pathway by analysis of expression kinetics from living bacteria.
868 Science *292*, 2080-2083.
869 Kato, M., Yano, K., Matsuo, F., Saito, H., Katagiri, T., Kurumizaka, H., Yoshimoto, M., Kasumi, F.,
870 Akiyama, F., Sakamoto, G.*, et al.* (2000). Identification of Rad51 alteration in patients with bilateral
871 breast cancer. J Hum Genet *45*, 133-137.
872 Kenyon, C.J., and Walker, G.C. (1980). DNA-damaging agents stimulate gene expression at specific loci
873 in Escherichia coli. Proc Natl Acad Sci U S A *77*, 2819-2823.
874 Kidane, D., and Graumann, P.L. (2005). Dynamic formation of RecA filaments at DNA double strand
875 break repair centers in live cells. J Cell Biol *170*, 357-366.
876 Kim, T., Chitteni-Pattu, S., Cox, B.L., Wood, E.A., Sandler, S.J., and Cox, M.M. (2015). Directed Evolution
877 of RecA Variants with Enhanced Capacity for Conjugational Recombination. PLoS genetics *11*,
878 e1005278.
879 Kowalczykowski, S.C. (2000). Initiation of genetic recombination and recombination-dependent
880 replication. Trends Biochem Sci *25*, 156-165.
881 Kuzminov, A. (1995). Collapse and repair of replication forks in Escherichia coli. Mol Microbiol *16*, 373-
882 384.
883 Lenhart, J.S., Brandes, E.R., Schroeder, J.W., Sorenson, R.J., Showalter, H.D., and Simmons, L.A. (2014).
884 RecO and RecR are necessary for RecA loading in response to DNA damage and replication fork stress.
885 Journal of bacteriology *196*, 2851-2860.
886 Lesterlin, C., Ball, G., Schermelleh, L., and Sherratt, D.J. (2014). RecA bundles mediate homology
887 pairing between distant sisters during DNA break repair. Nature *506*, 249-253.
888 Lestini, R., and Michel, B. (2007). UvrD controls the access of recombination proteins to blocked
889 replication forks. EMBO J *26*, 3804-3814.

890 Levin-Zaidman, S., Frenkiel-Krispin, D., Shimoni, E., Sabanay, I., Wolf, S.G., and Minsky, A. (2000).
891 Ordered intracellular RecA-DNA assemblies: a potential site of in vivo RecA-mediated activities. Proc
892 Natl Acad Sci U S A *97*, 6791-6796.
893 Little, J.W. (1982). Control of the SOS regulatory system by the level of RecA protease. Biochimie *64*,
894 585-589.
895 Little, J.W., and Mount, D.W. (1982). The SOS regulatory system of Escherichia coli. Cell *29*, 11-22.
896 Little, J.W., Mount, D.W., and Yanisch-Perron, C.R. (1981). Purified lexA protein is a repressor of the
897 recA and lexA genes. Proc Natl Acad Sci U S A *78*, 4199-4203.
898 Luo, Y., Pfuetzner, R.A., Mosimann, S., Paetzel, M., Frey, E.A., Cherney, M., Kim, B., Little, J.W., and
899 Strynadka, N.C. (2001). Crystal structure of LexA: a conformational switch for regulation of self-
900 cleavage. Cell *106*, 585-594.
901 Lusetti, S.L., and Cox, M.M. (2002). The bacterial RecA protein and the recombinational DNA repair of
902 stalled replication forks. Annu Rev Biochem *71*, 71-100.
903 Lusetti, S.L., Drees, J.C., Stohl, E.A., Seifert, H.S., and Cox, M.M. (2004a). The DinI and RecX proteins
904 are competing modulators of RecA function. J Biol Chem *279*, 55073-55079.
905 Lusetti, S.L., Shaw, J.J., and Cox, M.M. (2003a). Magnesium ion-dependent activation of the RecA
906 protein involves the C terminus. J Biol Chem *278*, 16381-16388.
907 Lusetti, S.L., Voloshin, O.N., Inman, R.B., Camerini-Otero, R.D., and Cox, M.M. (2004b). The DinI protein
908 stabilizes RecA protein filaments. J Biol Chem *279*, 30037-30046.
909 Lusetti, S.L., Wood, E.A., Fleming, C.D., Modica, M.J., Korth, J., Abbott, L., Dwyer, D.W., Roca, A.I.,
910 Inman, R.B., and Cox, M.M. (2003b). C-terminal deletions of the Escherichia coli RecA protein.
911 Characterization of in vivo and in vitro effects. J Biol Chem *278*, 16372-16380.
912 Markham, B.E., Little, J.W., and Mount, D.W. (1981). Nucleotide sequence of the lexA gene of
913 Escherichia coli K-12. Nucleic Acids Res *9*, 4149-4161.
914 Ndjonka, D., and Bell, C.E. (2006). Structure of a hyper-cleavable monomeric fragment of phage
915 lambda repressor containing the cleavage site region. J Mol Biol *362*, 479-489.
916 Ouzounov, N., Nguyen, J.P., Bratton, B.P., Jacobowitz, D., Gitai, Z., and Shaevitz, J.W. (2016). MreB
917 Orientation Correlates with Cell Diameter in Escherichia coli. Biophys J *111*, 1035-1043.
918 Park, J., Myong, S., Niedziela-Majka, A., Lee, K.S., Yu, J., Lohman, T.M., and Ha, T. (2010). PcrA helicase
919 dismantles RecA filaments by reeling in DNA in uniform steps. Cell *142*, 544-555.
920 Petrova, V., Chen, S.H., Molzberger, E.T., Tomko, E., Chitteni-Pattu, S., Jia, H., Ordabayev, Y., Lohman,
921 T.M., and Cox, M.M. (2015). Active displacement of RecA filaments by UvrD translocase activity.
922 Nucleic Acids Res *43*, 4133-4149.
923 Prakash, R., Zhang, Y., Feng, W., and Jasin, M. (2015). Homologous recombination and human health:
924 the roles of BRCA1, BRCA2, and associated proteins. Cold Spring Harb Perspect Biol *7*, a016600.
925 Ptashne, M., Jeffrey, A., Johnson, A.D., Maurer, R., Meyer, B.J., Pabo, C.O., Roberts, T.M., and Sauer,
926 R.T. (1980). How the lambda repressor and cro work. Cell *19*, 1-11.
927 Rajendram, M., Zhang, L., Reynolds, B.J., Auer, G.K., Tuson, H.H., Ngo, K.V., Cox, M.M., Yethiraj, A., Cui,
928 Q., and Weibel, D.B. (2015). Anionic Phospholipids Stabilize RecA Filament Bundles in Escherichia coli.
929 Mol Cell *60*, 374-384.
930 Ramirez, B.E., Voloshin, O.N., Camerini-Otero, R.D., and Bax, A. (2000). Solution structure of DinI
931 provides insight into its mode of RecA inactivation. Protein Sci *9*, 2161-2169.
932 Renzette, N., Gumlaw, N., Nordman, J.T., Krieger, M., Yeh, S.P., Long, E., Centore, R., Boonsombat, R.,
933 and Sandler, S.J. (2005). Localization of RecA in Escherichia coli K-12 using RecA-GFP. Mol Microbiol
934 *57*, 1074-1085.
935 Renzette, N., Gumlaw, N., and Sandler, S.J. (2007). DinI and RecX modulate RecA-DNA structures in
936 Escherichia coli K-12. Mol Microbiol *63*, 103-115.
937 Reyes-Lamothe, R., Sherratt, D.J., and Leake, M.C. (2010). Stoichiometry and architecture of active
938 DNA replication machinery in Escherichia coli. Science *328*, 498-501.
939 Roberts, J.W., and Roberts, C.W. (1975). Proteolytic cleavage of bacteriophage lambda repressor in
940 induction. Proc Natl Acad Sci U S A *72*, 147-151.

941 Robinson, A., McDonald, J.P., Caldas, V.E., Patel, M., Wood, E.A., Punter, C.M., Ghodke, H., Cox, M.M.,
942 Woodgate, R., Goodman, M.F.*, et al.* (2015). Regulation of Mutagenic DNA Polymerase V Activation in
943 Space and Time. PLoS genetics *11*, e1005482.
944 Ronen, M., Rosenberg, R., Shraiman, B.I., and Alon, U. (2002). Assigning numbers to the arrows:
945 parameterizing a gene regulation network by using accurate expression kinetics. Proc Natl Acad Sci U
946 S A *99*, 10555-10560.
947 Rupp, W.D., and Howard-Flanders, P. (1968). Discontinuities in the DNA synthesized in an excision-
948 defective strain of Escherichia coli following ultraviolet irradiation. J Mol Biol *31*, 291-304.
949 Salles, B., and Paoletti, C. (1983). Control of UV induction of recA protein. Proc Natl Acad Sci U S A *80*,
950 65-69.
951 San Filippo, J., Sung, P., and Klein, H. (2008). Mechanism of eukaryotic homologous recombination.
952 Annu Rev Biochem *77*, 229-257.
953 Sassanfar, M., and Roberts, J.W. (1990). Nature of the SOS-inducing signal in Escherichia coli. The
954 involvement of DNA replication. J Mol Biol *212*, 79-96.
955 Sauer, R.T., Ross, M.J., and Ptashne, M. (1982). Cleavage of the lambda and P22 repressors by recA
956 protein. J Biol Chem *257*, 4458-4462.
957 Stasiak, A., and Egelman, E.H. (1986). Structure and Dynamics of recA Protein-DNA Complexes as
958 Determined by Image Analysis of Electron Micrographs. Biophys J *49*, 5-7.
959 Stayrook, S., Jaru-Ampornpan, P., Ni, J., Hochschild, A., and Lewis, M. (2008). Crystal structure of the
960 lambda repressor and a model for pairwise cooperative operator binding. Nature *452*, 1022-1025.
961 Stohl, E.A., Brockman, J.P., Burkle, K.L., Morimatsu, K., Kowalczykowski, S.C., and Seifert, H.S. (2003).
962 Escherichia coli RecX inhibits RecA recombinase and coprotease activities in vitro and in vivo. J Biol
963 Chem *278*, 2278-2285.
964 Sung, P. (1994). Catalysis of ATP-dependent homologous DNA pairing and strand exchange by yeast
965 RAD51 protein. Science *265*, 1241-1243.
966 Uhlin, B.E., Volkert, M.R., Clark, A.J., Sancar, A., and Rupp, W.D. (1982). Nucleotide sequence of a recA
967 operator mutation. LexA/operator-repressor binding/inducible repair. Mol Gen Genet *185*, 251-254.
968 Veaute, X., Delmas, S., Selva, M., Jeusset, J., Le Cam, E., Matic, I., Fabre, F., and Petit, M.A. (2005).
969 UvrD helicase, unlike Rep helicase, dismantles RecA nucleoprotein filaments in Escherichia coli. EMBO
970 J *24*, 180-189.
971 Volkert, M.R., George, D.L., and Witkin, E.M. (1976). Partial suppression of the LexA phenotype by
972 mutations (rnm) which restore ultraviolet resistance but not ultraviolet mutability to Escherichia coli
973 B/r uvr A lexA. Mutat Res *36*, 17-28.
974 Walker, G.C. (2001). To cleave or not to cleave? Insights from the LexA crystal structure. Mol Cell *8*,
975 486-487.
976 Yeeles, J.T., and Marians, K.J. (2013). Dynamics of leading-strand lesion skipping by the replisome. Mol
977 Cell *52*, 855-865.
978 Yu, X., and Egelman, E.H. (1993). The LexA repressor binds within the deep helical groove of the
979 activated RecA filament. J Mol Biol *231*, 29-40.
980 Zaslaver, A., Bren, A., Ronen, M., Itzkovitz, S., Kikoin, I., Shavit, S., Liebermeister, W., Surette, M.G.,
981 and Alon, U. (2006). A comprehensive library of fluorescent transcriptional reporters for Escherichia
982 coli. Nat Methods *3*, 623-628.

983